

A Natural origin for the LHCb anomalies

Eugenio Megías^a, Giuliano Panico^b, Oriol Pujolàs^b, Mariano Quirós^{b,c}

^a*Max-Planck-Institut für Physik (Werner-Heisenberg-Institut),
Föhringer Ring 6, D-80805, Munich, Germany*

^b*Institut de Física d'Altes Energies (IFAE),
The Barcelona Institute of Science and Technology (BIST),
Campus UAB, 08193 Bellaterra (Barcelona) Spain*

^c*ICREA, Pg. Lluís Companys 23, 08010 Barcelona, Spain*

Abstract

The anomalies recently found by the LHCb collaboration in B -meson decays seem to point towards the existence of new physics coupled non-universally to muons and electrons. We show that a beyond-the-Standard-Model dynamics with these features naturally arises in models with a warped extra-dimension that aim to solve the electroweak Hierarchy Problem. The attractiveness of our set-up is the fact that the dynamics responsible for generating the flavor anomalies is automatically present, being provided by the massive Kaluza–Klein excitations of the electroweak gauge bosons. The flavor anomalies can be easily reproduced by assuming that the bottom and muon fields have a sizable amount of compositeness, while the electron is almost elementary. Interestingly enough, this framework correlates the flavor anomalies to a pattern of corrections in the electroweak observables and in flavor-changing processes. In particular the deviations in the bottom and muon couplings to the Z -boson and in $\Delta F = 2$ flavor-changing observables are predicted to be close to the present experimental bounds, and thus potentially testable in near-future experiments.

Contents

1	Introduction	3
2	The model	4
3	The $B \rightarrow K^* \mu^+ \mu^-$ anomaly	11
4	Constraints	15
4.1	General overview	15
4.2	Electroweak precision data	18
4.2.1	Oblique corrections	19
4.2.2	The $Z\bar{b}b$ coupling	20
4.2.3	The $Z\bar{\mu}\mu$ coupling	23
4.3	Flavor observables	24
4.4	The ATLAS di-muon resonance search	25
4.5	Direct searches on KK gluons	26
5	Conclusions	28

1 Introduction

After the discovery of a Higgs-like particle at the LHC, the Electroweak (EW) Hierarchy Problem became arguably one of the most pressing theoretical issues in high-energy particle physics. Although several motivated extensions of the Standard Model (SM) have been proposed to address this issue, no unambiguous experimental evidence is yet available to clearly discriminate among the various theoretical possibilities.

A straightforward way to hunt for a Beyond the SM (BSM) dynamics is to use direct searches of new resonances at the LHC. This strategy is quite powerful in probing BSM scenarios that connect the solution of the Hierarchy Problem to the presence of new light states (around $1 - 2$ TeV), as for instance models based on Supersymmetry or on the composite Higgs idea. Specific scenarios, however, could evade this strong connection and push the new states into the multi-TeV range as a consequence of either a peculiar structure of the BSM dynamics or of a mild amount of fine-tuning. In such situation, direct searches may have a hard time in successfully testing the BSM effects.

An additional, complementary approach to gain experimental information on BSM scenarios is to exploit indirect searches, which in several cases are sensitive to new-physics scales much higher than the TeV. Noticeable examples are the EW precision measurements performed at LEP and the flavor observables, in particular flavor-changing and/or CP violating processes. The latter observables, for instance, are able to probe new-physics effects suppressed by energy scales as high as 10^5 TeV. As can be easily understood, indirect searches can be extremely important to probe scenarios with a high new-physics scale. However they retain their relevance also in scenarios with relatively light new resonances, since they can provide complementary constraints on the parameter space of the models.

Indirect searches can also provide some evidence for new phenomena and give some indication of the possible BSM models that could explain them. An intriguing example are the anomalies in the B -meson decays recently found at the LHCb [1, 2] and Belle [3] experiments. In particular the ratio of branching fractions $\text{BR}(B \rightarrow K\mu^+\mu^-)/\text{BR}(B \rightarrow Ke^+e^-)$, which differs from the SM prediction at the 2.6σ level, could be suggestive of a violation of universality in the lepton sector. Several theoretical analyses already appeared in the literature trying to interpret the anomalies in a BSM perspective. The most obvious possibilities are some extensions of the SM including massive vector bosons (Z') [4–6], or new resonances with mixed couplings to quarks and leptons (leptoquarks) [7], although it might also be due to underestimated hadronic uncertainties [8]. A shortcoming of many of these constructions is the fact that the BSM dynamics has no fundamental reason for being present, other than explaining the anomalies in B meson physics. In the present work we follow a different approach: we do not add ad-hoc new states in order to fit the data, but instead we try to connect the LHCb anomaly to some BSM dynamics whose main motivation is addressing the EW Hierarchy Problem.

A natural way to achieve this aim is to consider extra-dimensional models a la Randall–Sundrum (RS) [9]. In these scenarios new massive vector bosons arise automatically as Kaluza–Klein (KK) modes of the SM gauge fields. In particular, the KK towers of the Z boson and of the photon can give rise to effective four-fermion interactions that modify the B -meson decays. A necessary requirement to get large enough effects is the assumption that the bottom quark and the muon have a non-negligible amount of compositeness ¹, i.e. that their wave-functions are sufficiently localized towards the IR, such that their couplings with the KK vector modes are large.

An interesting byproduct of this set-up is the fact that additional corrections to precision observables are necessarily generated as a consequence of the bottom and muon compositeness. Among the most relevant effects we can mention the distortions of the bottom and the muon couplings to the Z -boson and the generation of $\Delta F = 2$ flavor-violating contact operators. As we will discuss in Sect. 4, in Natural scenarios that solve the Hierarchy Problem, an explanation of the LHCb anomaly is correlated with deviations in the Z couplings and $\Delta F = 2$ effects that are close to present experimental bounds. This correlation leads to a very predictive set-up, in which the main parameters of the extra-dimensional model are almost completely fixed.

For definiteness, in our analysis we focus on a simple modification of the classical RS set-up, obtained by a soft-wall-like deformation of the AdS metric close to the IR brane [10–19]. This modified scenario allows to keep under control the corrections to the EW precision parameters even in the absence of a custodial symmetry in the bulk. In this way the strong constraints on the mass scale of the KK vector fields can be relaxed to the ~ 2 TeV range, thus avoiding the presence of a Little Hierarchy Problem between the EW scale and the KK scale.

The paper is organized as follows. In Sect. 2, we present a brief overview of our model, summarizing the main results of the existing literature. Afterwards, in Sect. 3, we analyze the new-physics effects in the B -meson decays and we determine the values of the parameters that allow to fit the present experimental data. The constraints coming from EW precision measurements, flavor observables and direct searches are then presented in Sect. 4. Finally in Sect. 5, we combine the fit of the LHCb anomaly and the experimental constraints, presenting an overall picture of the viability of our model together with a few concluding remarks.

2 The model

In this section we will present the model we will use in the rest of the work for our analysis of the B -meson decay anomalies. As mentioned in the Introduction, the scenario

¹The role of left-handed muon compositeness in deviations from lepton flavor universality has been recently considered in Ref. [5] in composite Higgs models with custodial protection.

we focus on is analogous to the usual RS set-up, the only difference being a deformation of the background metric near the infrared (IR) boundary. The extra-dimension is thus close to AdS₅ near the ultraviolet (UV) brane, whereas the conformal invariance is broken by a deformation of the metric only near the IR. This structure guarantees that the RS explanation of the hierarchy between the UV and IR scales is still at work in our model, so that fields localized near the IR brane (most noticeably the Higgs) “feel” an effective cut-off scale of TeV order. A detailed discussion of the model can be found in Ref. [18], to which we refer the reader for further details.

In the following we will denote by y the proper coordinate along the extra dimension and by $A(y)$ the warp factor defining the metric

$$ds^2 = e^{-2A(y)} \eta_{\mu\nu} dx^\mu dx^\nu + dy^2, \quad (2.1)$$

where $\eta_{\mu\nu} = (-1, 1, 1, 1)$. The UV and IR branes are localized at the points $y = 0$ and $y = y_1$ respectively. The form of the warp factor is determined by the dynamics of the scalar field ϕ which stabilizes the length of extra dimension. We assume its dynamics to be characterized by the superpotential

$$W(\phi) = 6k (1 + e^{a\phi})^b, \quad (2.2)$$

where a and b are real (dimensionless) parameters controlling the gravitational background and k is a parameter with mass dimension related to the curvature along the fifth dimension [10]. Since a one-to-one correspondence is present between the value of the ϕ field and the position along the extra dimension, it is possible to trade the coordinate y for the value of ϕ . From the superpotential we extract the explicit form of the warp factor

$$A(\phi) = B(\phi) - B(\phi_0), \quad B(\phi) = \frac{1}{6ab} \left(\phi - \frac{e^{-a\phi}}{a} \right). \quad (2.3)$$

In ϕ coordinates the brane locations correspond to ϕ_0 and ϕ_1 for the UV and IR branes, respectively. We fix throughout the paper $\phi_1 = 5$, while the position of the UV brane ϕ_0 is used to fix the length of the extra dimension [18]. Equivalently, setting the length of the extra dimension corresponds to fixing the value of $A_1 = A(\phi_1)$ at the IR brane.

We assume that a five-dimensional (5D) gauge invariance is present, whose gauge group coincides with the SM one $SU(2)_L \times U(1)_Y \times SU(3)_c$. We denote the corresponding gauge fields as $W_M^a(x, y)$, $B_M(x, y)$, $G_M^A(x, y)$, where $M = (\mu, 5)$, $a = 1, 2, 3$ and $A = 1, \dots, 8$. The gauge fields can be decomposed in KK modes as $A_\mu(x, y) = \sum_n f_A^{(n)}(y) A_\mu^n(x) / \sqrt{y_1}$. The profiles $f_A^{(n)}(y)$, normalized as $\int_0^{y_1} \left(f_A^{(n)}(y) \right)^2 = y_1$, satisfy Neumann boundary conditions and bulk equations of motion

$$\left(m_A^{(n)} \right)^2 f_A^{(n)} + \left(e^{-2A} \dot{f}_A^{(n)} \right)' - M_A^2(y) f_A^{(n)} = 0, \quad (2.4)$$

where we use the notation $\dot{X} \equiv dX/dy$, while $m_A^{(n)}$ denotes the mass of the n -th KK mode and $M_A(y)$ is the mass term induced by the vacuum expectation value of the Higgs after EW symmetry breaking (EWSB). For a Higgs propagating in the bulk, as we will assume in the following, the mass terms $M_A(y)$ has the form

$$M_W(y) = \frac{g_5}{2} h(y) e^{-A(y)}, \quad M_Z(y) = \frac{1}{c_W} M_W(y), \quad (2.5)$$

where $h(y)$ is the Higgs background profile and g_5 denotes the 5D gauge coupling corresponding to the $SU(2)_L$ subgroup. The g_5 coupling is related to the usual four-dimensional (4D) one, g , by $g_5 = g\sqrt{y_1}$. For illustration, we plot the profiles $f_A^{(n)}$ for $n = 1, 2$ in the left panel of Fig. 1 for the benchmark configuration with superpotential parameters $b = 1$ and $a = 0.2$ and with $A_1 = 35$. We will use this choice of parameters throughout the paper to derive all the numerical results. In addition we will also assume that the mass of the first gauge KK mode is of order $m_{KK} \equiv M_1 \simeq 2$ TeV. This choice for the KK mass corresponds to the lowest value compatible with the EW precision measurements, in particular with the bounds on the S and T parameters, and with the direct LHC searches as we will discuss in Sects. 4.2.1 and 4.5.

Notice that the KK modes profiles before EWSB are universal, i.e. they do not depend on the specific gauge field they belong to. After the Higgs gets a vacuum expectation value and the $M_A(y)$ mass turns on for the W and Z bosons, mild non-universal deformations of the KK wave-functions are induced. These deformations are however typically negligible for most of the computations we perform in our paper since the KK mass scale is much larger than the EW scale $v \simeq 246$ GeV.

Let us now consider the Higgs field. As we already mentioned, we assume it to be a 5D field, so that it propagates in the bulk. Splitting the degrees of freedom into Goldstone modes $\chi(x, y)$, vacuum expectation (background) value $h(y)$ and physical fluctuations $\xi(x, y)$ we can rewrite the Higgs field as

$$H(x, y) = \frac{1}{\sqrt{2}} e^{i\chi(x, y)} \begin{pmatrix} 0 \\ h(y) + \xi(x, y) \end{pmatrix}. \quad (2.6)$$

EWSB is triggered by an IR brane potential, whereas additional mass terms are introduced for the Higgs in the bulk and at the UV brane. The full Higgs potential is

$$V(H) = M^2(\phi) |H|^2 + M_0 |H|^2 \delta(y) + (-M_1 |H|^2 + \gamma |H|^4) \delta(y - y_1), \quad (2.7)$$

where

$$M^2(\phi) = \alpha k \left[\alpha k - \frac{2}{3} W(\phi) \right]. \quad (2.8)$$

The dimensionless parameter α controls the localization of the Higgs wavefunction and can thus be connected to the amount of tuning related to the Hierarchy Problem ².

²In a purely AdS metric, solving the Hierarchy Problem requires $\alpha \geq 2$. See e.g. Ref. [20].

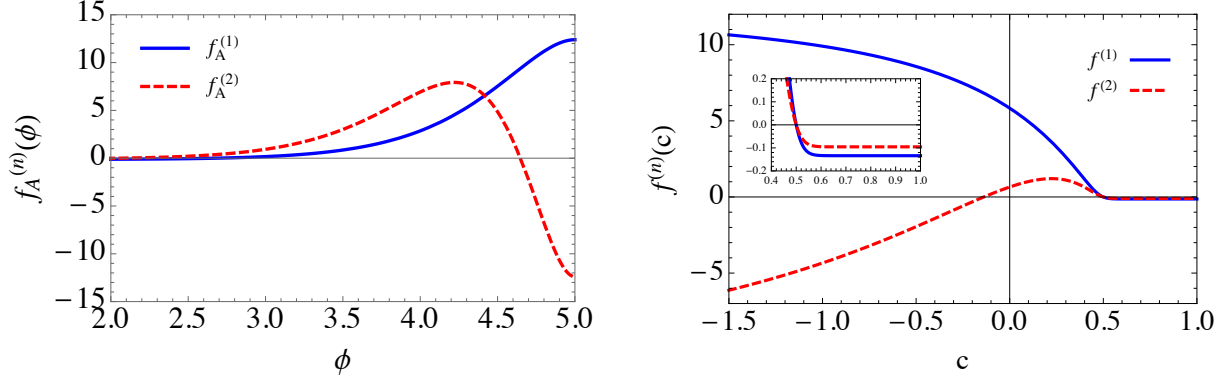


Figure 1: *Left panel: Profiles of the gauge boson KK modes $f_A^{(n)}$ for $n = 1, 2$ (solid blue and dashed red lines respectively). These modes actually extend from $\phi_0 = -8.94$ to $\phi_1 = 5$, but we display only the region $\phi \geq 2$ to better visualize the non-trivial behavior close to the IR brane. In the region approaching the UV brane the modes are approximately constant with values $f_A^{(1)} \simeq -0.1339$ and $f_A^{(2)} \simeq -0.0954$. Right panel: Coupling (normalized with respect to the 4D coupling g) of a fermion zero-mode with the n -th KK gauge field, $f^{(n)}(c)$, as a function of the fermion localization parameter c (cf. Eq. (2.17)). The solid blue and dashed red lines correspond to the coupling with the first and second gauge KK modes, respectively.*

In fact in order to ensure that the Higgs background $h(y)$ has the required exponential shape

$$h(y) = h(0)e^{\alpha ky} \quad (2.9)$$

a certain relation must be satisfied between the UV mass and the bulk potential, namely $M_0 = \alpha k + \Delta M_0$ with [17]

$$\frac{\Delta M_0}{M_0} = \frac{1}{\alpha k \int_0^{y_1} dy e^{4A-2\alpha ky}}. \quad (2.10)$$

Obviously if ΔM_0 is required to be much smaller than M_0 and αk , an amount of fine-tuning of order $\Delta M_0/M_0$ is present in the model. The integrand in the denominator of Eq. (2.10) is a monotonously increasing function of y and it can be easily checked that the fine-tuning is avoided for large enough values of α

$$\alpha \gtrsim \alpha_1 = \frac{2A_1}{ky_1}, \quad (2.11)$$

which correspond to localizing the Higgs background profile towards the IR brane. For smaller values of α ($\alpha < \alpha_1$) some degree of fine-tuning is needed as shown in the left panel of Fig. 2 where we plot $\Delta M_0/M_0$ versus α for values of $\alpha \leq \alpha_1$ (for our choice of superpotential parameters we find $\alpha_1 \simeq 3.2$). We can see that the tuning is essentially absent for $\alpha \gtrsim 2.95$, whereas it increases exponentially for smaller values of α .

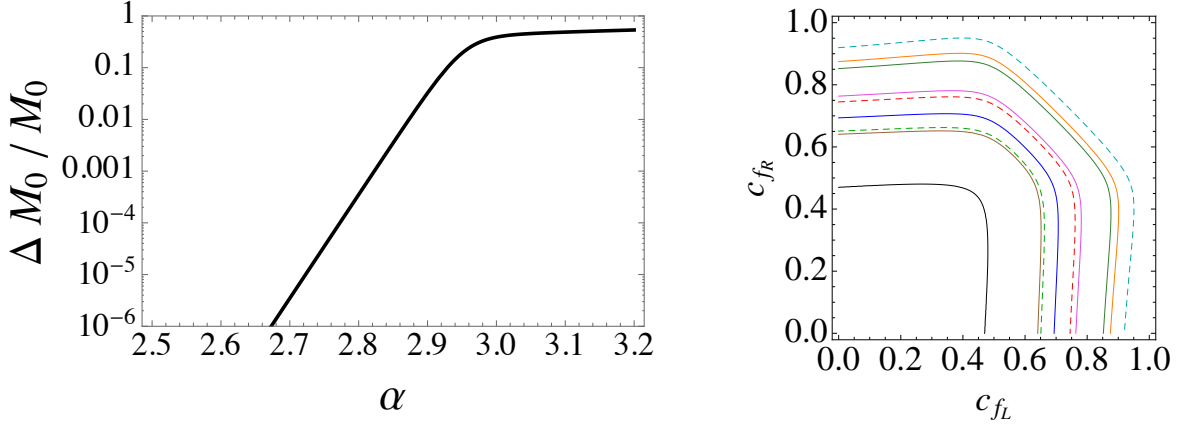


Figure 2: *Left panel: Amount of tuning $\Delta M_0/M_0$ as a function of α . Right panel: Regions in the plane (c_{f_L}, c_{f_R}) that accommodate the masses of the quarks and leptons. The various contours (from the outermost to the innermost) correspond to electron, up, down, strange, muon, charm, tau lepton, bottom and top. As explained in the main text, in the numerical results we included the QCD running effects for the quark masses up to the KK mass scale $m_{KK} \sim 2$ TeV. In the parameter space region inside each contour the mass of the corresponding fermion can be obtained for values of the Yukawa couplings $\sqrt{k}\hat{Y}_{ij}^q \leq 3$.*

The SM fermions are realized in our scenario as chiral zero modes of 5D fermions. The localization of the different fermions is determined by the 5D mass terms. The mass term for the 5D fermions can be conveniently chosen as $M_{f_{L,R}}(y) = \mp c_{f_{L,R}} W(\phi)$ where the upper (lower) sign applies for a field with a left-handed (right-handed) zero mode [16]. With this convention the fermion zero modes are localized near the UV (IR) brane for $c_{f_{L,R}} > 1/2$ ($c_{f_{L,R}} < 1/2$). A value $c_{f_{L,R}} < 1/2$ thus corresponds to a sizable amount of compositeness for the corresponding fermions, whereas $c_{f_{L,R}} > 1/2$ characterizes fermions that are almost elementary. Choosing appropriate boundary conditions we can ensure that each 5D fermion has a massless zero mode with the appropriate chirality, whose wave-function is

$$\psi_{L,R}^{(0)}(y, x) = \frac{e^{(2-c_{L,R})A(y)}}{\left(\int dy e^{A(1-2c_{L,R})}\right)^{1/2}} \psi_{L,R}(x). \quad (2.12)$$

Yukawa interactions with the Higgs are induced by the following Lagrangian

$$\mathcal{L}_Y = \hat{Y}_{ij}^u \tilde{H} \bar{Q}_L^i u_R^j + \hat{Y}_{ij}^d H \bar{Q}_L^i d_R^j + \hat{Y}_{ij}^e H \bar{\ell}_L^i e_R^j, \quad (2.13)$$

where \hat{Y}_{ij}^f are 5D Yukawa couplings with mass dimension $-1/2$. The dimensionless 4D

Yukawa couplings are then given by

$$Y_{ij}^f = \sqrt{k} \hat{Y}_{ij}^f F(c_{QL}, c_{qR}), \quad F(c_L, c_R) = \frac{\int h e^{-(c_L+c_R)A}}{\left[\int h^2 e^{-2A} \int e^{(1-2c_L)A} \int e^{(1-2c_R)A} \right]^{1/2}}. \quad (2.14)$$

As can be seen from the above formulae, analogously to what happens in the usual RS set-up, order-one differences in the fermion bulk masses (i.e. in the $c_{f_{L,R}}$ parameters) induce exponential differences in the fermion Yukawa's. This mechanism could be interpreted as a natural way to generate the hierarchies in the fermion masses, without any need to introduce hierarchies in the 5D Yukawa's. This set-up is usually called anarchic flavor scenario since the 5D Yukawa's have an ‘‘anarchic’’ structure with all entries of similar order³. In the present work we do not fully specify the flavor structure of the model and we just consider the coefficients $c_{f_{L,R}}$ as free parameters such that for ‘‘perturbative’’ values of the Yukawa coefficients \hat{Y}_{ij}^f the SM fermion masses and mixing angles can be reproduced. In other words, differently from the pure anarchic scenario, in our set-up we also allow for some (mild) hierarchy in the 5D Yukawa's which should arise from some 5D flavor structure.

Since the quark and charged lepton spectrum is hierarchical, a good approximation to extract the fermion masses as a function of the model parameters is to neglect the mixing angles (which means that $\hat{Y}_{ij}^f \sim 0$ for $i \neq j$). In this way we can easily determine the range of values of $c_{f_{L,R}}$ that allow to reproduce the various fermion masses. The numerical results, corresponding to a benchmark choice of the 5D Yukawa couplings, $\sqrt{k} \hat{Y}_{ii}^f = 3$, are shown in the right panel of Fig. 2. In the analysis we used the values of the SM quark Yukawa couplings run at the energy scale of the KK resonances in our model, namely $m_{KK} \sim 2$ TeV,

$$m_t(m_{KK}) \simeq 140 \text{ GeV}, \quad m_b(m_{KK}) \simeq 2.3 - 2.5 \text{ GeV}, \quad m_c(m_{KK}) \simeq 0.43 - 0.55 \text{ GeV}, \\ m_s(m_{KK}) \simeq 28 - 81 \text{ MeV}, \quad m_u(m_{KK}) \simeq 1 - 2 \text{ MeV}, \quad m_d(m_{KK}) \simeq 1 - 4 \text{ MeV}. \quad (2.15)$$

Another important ingredient we will need for our analysis is the coupling of the SM fermions with the KK modes of the gauge fields. Before EWSB these couplings have a particularly simple form. Obviously the ones with the SM gauge bosons coincide with the SM gauge couplings. The couplings with the massive gauge KK modes are instead universal and are fully determined by the localization of the fermions, i.e. by the $c_{f_{L,R}}$ parameters. The coupling with the n -th gauge KK modes, collectively denoted by X_μ^n , can be written as

$$g_{f_{L,R}}^{X^n} X_\mu^n \bar{f}_{L,R} \gamma^\mu f_{L,R} \equiv g f^{(n)}(c_{f_{L,R}}) X_\mu^n \bar{f}_{L,R} \gamma^\mu f_{L,R}, \quad (2.16)$$

³For the original papers on the anarchic flavor scenario in 5D warped models see Refs. [21]. For the analogous construction in the context of the 4D interpretation of the extra-dimensional models see for instance Ref. [22].

where $f_{L,R}$ are the fermion zero-mode and g denotes the SM gauge coupling corresponding to the X_μ field. The coupling functions $f^{(n)}(c_{f_{L,R}})$, which encode the overlap of the KK wave-functions of the vector bosons with the zero-mode fermion wave-functions, are given by the following expression

$$f^{(n)}(c) = \frac{\sqrt{y_1}}{\sqrt{\int_0^{y_1} (f_A^{(n)}(y))^2}} \frac{\int_0^{y_1} f_A^{(n)}(y) e^{(1-2c)A(y)}}{\int_0^{y_1} e^{(1-2c)A(y)}}. \quad (2.17)$$

The functions $f^{(n)}(c)$ for $n = 1, 2$ for our reference choice of the model parameters are plotted in the right panel of Fig. 1. We can see that two relevant regimes are present. For a fermion zero mode localized towards the IR (namely for $c \lesssim 0.45$) the coupling with the KK gauge fields is typically of the order of the SM gauge coupling (that is $f^{(n)}(c) \sim 1$) and can become even stronger for $c \lesssim 0$. For fields which are almost elementary (namely for $c \gtrsim 0.5$) the coupling instead becomes rather weak with a typical size $\sim 0.1g$ ⁴.

It is interesting to notice that, for fermions with very small compositeness, the coupling with the gauge KK's becomes almost independent of the exact value of c . One can indeed check that for arbitrary $c_1, c_2 \gtrsim 0.6$ the couplings differ at most at the percent level, $|f^{(n)}(c_1) - f^{(n)}(c_2)| / |f^{(n)}(c_1)| \lesssim 10^{-2}$. This feature has very important consequences for flavor universality. Indeed gauge coupling universality is automatically ensured for all the fermions whose localization parameters are $c_{f_{L,R}} \gtrsim 0.6$. In the following we will exploit this feature by assuming that the first and second quark generations respect the universality condition. This implies an approximate accidental $U(2)_{q_L} \times U(2)_{u_R} \times U(2)_{d_R}$ global flavor symmetry, which is only broken by the Yukawa couplings. As we will see this symmetry will help in reducing dangerous flavor violating effects involving the light quarks⁵. As can be seen from Fig. 2 there is no obstruction in satisfying the universality assumption since the Yukawa couplings of the first two generations of quarks can be easily accommodated by choosing $c_{f_L} \sim c_{f_R} \gtrsim 0.6$. For simplicity in our numerical analysis we will moreover choose $c_{q_L^1} = c_{q_L^2} \equiv c_{q_L}$ (where $q_L^{1,2}$ denote the left-handed quark doublets in the first and second generation) as well as $c_{u_R} = c_{c_R} = c_{d_R} = c_{s_R} \equiv c_{q_R}$. This choice is not strictly necessary, since any configuration which respects $c_{f_{L,R}} \gtrsim 0.6$ would give rise to the effective $U(2)$ flavor invariance.

The results about the couplings with the KK gauge tower we presented so far are exact when the effects of EWSB are neglected. When the Higgs gets a vacuum expectation value, however, some (possibly non-universal) distortions of the couplings are generated. There are two main effects that modify the gauge couplings: the mixing of the SM fermions

⁴For $c = 1/2$ all the couplings to the KK gauge modes exactly vanish as a consequence of the fact that the wave-functions of the fermion zero modes become flat along the extra dimension.

⁵Flavor models including an approximate $U(2)$ flavor invariance for the light generations have already been considered in the literature in the context of composite Higgs models. See for instance Refs. [23].

with their KK modes and the mixing of the SM gauge fields with the massive vector resonances. We postpone a detailed discussion of these effects to Sect. 4.

3 The $B \rightarrow K^* \mu^+ \mu^-$ anomaly

As we mentioned in the Introduction, the recent LHCb measurements of the angular distributions in the decay $B \rightarrow K^* \mu^+ \mu^-$ and the $\sim 2.6 \sigma$ deviation with respect to the SM prediction in the value of $BR(B \rightarrow K \mu^+ \mu^-)/BR(B \rightarrow K e^+ e^-) \simeq 0.745_{-0.074}^{+0.090} \pm 0.036$ [1] suggest the possibility that universality deviations with respect to the Standard Model expectations could be present. After EWSB the relevant four-fermion effective operators contributing to $\Delta F = 1$ transitions can be mapped into the basis [24]

$$\mathcal{L}_{eff} = \frac{G_F \alpha}{\sqrt{2} \pi} V_{ts}^* V_{tb} \sum_i C_i \mathcal{O}_i, \quad (3.1)$$

where the Wilson coefficients $C_i = C_i^{SM} + \Delta C_i$, are the sum of a SM contribution C_i^{SM} and of a new-physics one ΔC_i . The sum in Eq. (3.1) includes the operators ⁶

$$\begin{aligned} \mathcal{O}_9 &= (\bar{s}_L \gamma_\mu b_L) (\bar{\mu} \gamma^\mu \mu), & \mathcal{O}_{10} &= (\bar{s}_L \gamma_\mu b_L) (\bar{\mu} \gamma^\mu \gamma_5 \mu), \\ \mathcal{O}'_9 &= (\bar{s}_R \gamma_\mu b_R) (\bar{\mu} \gamma^\mu \mu), & \mathcal{O}'_{10} &= (\bar{s}_R \gamma_\mu b_R) (\bar{\mu} \gamma^\mu \gamma_5 \mu). \end{aligned} \quad (3.2)$$

In our model contact interactions involving the SM fermions can be generated through the exchange of the massive KK modes of the gauge fields. In particular interactions that induce $\Delta F = 1$ transitions can be induced by the exchange of the KK modes of the Z -boson and of the photon. The schematic structure of the diagrams giving rise to these contributions is shown in Fig. 3.

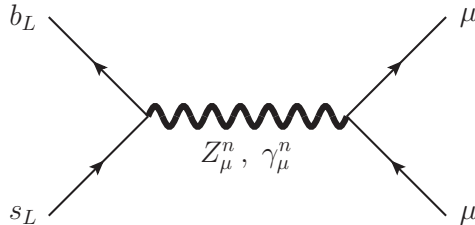


Figure 3: *Feynman diagrams giving rise to the effective operators of Eq. (3.2)*

From the discussion in the previous section, it is easy to realize that lepton universality can be broken in our scenario, provided that the localization of the various lepton generations is different. In particular, if the electron is an almost elementary state ($c_{e_{L,R}} \gtrsim 0.6$)

⁶Additional operators involving the electron field can also contribute to $\Delta F = 1$ processes. In our set-up, however, we assume that the first lepton generation is almost elementary, so that new contact interactions involving the electron are negligible.

whereas the muon has a sizable degree of compositeness, the couplings of these two fields to the gauge KK modes are different (see the right panel of Fig. 1). In this case large contributions to the $\Delta F = 1$ operators in Eq. (3.2) can be generated.

A set-up that allows to accommodate a large enough contribution to the $\Delta F = 1$ transitions is obtained by assuming that the left-handed component of the muon has a sizable degree of compositeness, $c_{\mu_L} \lesssim 0.5$. Analogously we also need to assume a large compositeness for at least one of the chiralities of the bottom quark. For the light generation quarks (as well as for the electron) we can instead assume a localization close to the UV brane, $c_{q_{L,R}} \gtrsim 0.6$, which realizes the approximate $U(2)$ quark flavor symmetry discussed in Sect. 2.

Before EWSB, the Lagrangian describing the interactions of the SM fermions with the vector KK modes can be written in the schematic form

$$\begin{aligned} \mathcal{L}_{EW} = \sum_{X=Z,\gamma} \frac{X_\mu^n}{2c_W} & \left[g_{b_L}^{X^n} \bar{b} \gamma_\mu (g_{b_L}^{X^n} P_L + g_{b_R}^{X^n} P_R) b + \sum_{q=u,d,c,s} (g_{q_L}^{X^n} \bar{q} \gamma_\mu P_L q + g_{q_R}^{X^n} \bar{q} \gamma_\mu P_R q) \right. \\ & \left. + \sum_{\ell=\mu,e} \bar{\ell} \gamma^\mu (g_{\ell_V}^{X^n} - g_{\ell_A}^{X^n} \gamma_5) \ell \right], \end{aligned} \quad (3.3)$$

where $P_{R,L} = (1 \pm \gamma_5)/2$ denote the right and left chirality projectors. After EWSB the off-diagonal Yukawa couplings induce a mixing between the fermions of the different generations, thus leading to flavor changing couplings to the Z and photon KK excitations. In our analysis we will assume that the unitary rotations that diagonalize the down quark Yukawa's have the same structure of the CKM matrix, $V_{L,R}^D \sim V_{CKM}$. Due to the larger hierarchy between the up quark-sector masses, we instead assume that the V^U rotation matrices are almost equal to the identity, $V_{L,R}^U \simeq \mathbf{1}_3$ ⁷. For the lepton sector we assume that the rotation matrices involving the charged leptons are close to the identity, so that flavor-violating interactions with the vector KK modes are not generated. We will not specify here how the required alignment in the lepton sector is achieved and we leave this point for future investigation.

With these assumptions, the leading flavor violating interactions with the vector KK modes have the form

$$\mathcal{L}_{EW} = \sum_{X=Z,\gamma} \frac{X_\mu^n}{2c_W} \left[V_{3i}^* V_{3j} \bar{d}_i \gamma^\mu \{ (g_{b_L}^{X^n} - \bar{g}_L^{X^n}) P_L + (g_{b_R}^{X^n} - \bar{g}_R^{X^n}) P_R \} d_j + \text{h.c.} \right], \quad (3.4)$$

where V_{ij} are the CKM matrix elements, d_i ($i = 1, 2, 3$) denotes the down-type quark in the i -th generation and $\bar{g}_{L,R}^{X^n}$ are the (universal) couplings of the first and second down quarks generation to the KK vectors. Notice that the Lagrangian in Eq. (3.4) has a

⁷Notice that the assumption $V_L^U \simeq \mathbf{1}_3$ implies that $V_L^D \simeq V_{CKM}$. However although the V_R^D rotation matrix is instead not fully fixed, for definiteness we identify it here with the CKM matrix as well. The main results we will derive depend only mildly on this assumption.

quite non-generic form, which closely resembles a minimal flavor violation structure in which all flavor-changing effects are suppressed by the CKM elements involving the third family. This is a direct consequence of the $U(2)$ flavor symmetry for the light generation quarks and of the unitarity of the CKM matrix. Would the $U(2)$ symmetry be violated, potentially large flavor-changing currents could be generated for the light quarks, and in particular $s \rightarrow d$ transitions could get sizable contributions.

The explicit expressions of the left- and right-handed couplings are

$$\begin{aligned} g_{f_L}^{Z^n} &= 2(t_{3L} - Q_f s_W^2) g f^{(n)}(c_{f_L}) & g_{f_L}^{\gamma^n} &= 2Q_f s_W c_W g f^{(n)}(c_{f_L}) \\ g_{f_R}^{Z^n} &= -2Q_f s_W^2 g f^{(n)}(c_{f_R}) & g_{f_R}^{\gamma^n} &= 2Q_f s_W c_W g f^{(n)}(c_{f_R}) \end{aligned} \quad (3.5)$$

From these expressions one can easily derive the vector and axial couplings, which we denote by $g_{f_{V,A}}^{X^n} = (g_{f_L}^{X^n} \pm g_{f_R}^{X^n})/2$.

The couplings in Eqs. (3.3) and (3.4) give rise to the following contributions to the Wilson coefficients of the $\Delta F = 1$ operators:

$$\begin{aligned} \Delta C_9 &= - \sum_{X=Z,\gamma} \sum_n \frac{\pi g_{\mu V}^{X^n} (g_{b_L}^{X^n} - g_{s_L}^{X^n})}{2\sqrt{2} G_F \alpha c_W^2 M_n^2}, & \Delta C'_9 &= - \sum_{X=Z,\gamma} \sum_n \frac{\pi g_{\mu V}^{X^n} (g_{b_R}^{X^n} - g_{s_R}^{X^n})}{2\sqrt{2} G_F \alpha c_W^2 M_n^2}, \\ \Delta C_{10} &= \sum_{X=Z,\gamma} \sum_n \frac{\pi g_{\mu A}^{X^n} (g_{b_L}^{X^n} - g_{s_L}^{X^n})}{2\sqrt{2} G_F \alpha c_W^2 M_n^2}, & \Delta C'_{10} &= \sum_{X=Z,\gamma} \sum_n \frac{\pi g_{\mu A}^{X^n} (g_{b_R}^{X^n} - g_{s_R}^{X^n})}{2\sqrt{2} G_F \alpha c_W^2 M_n^2}. \end{aligned} \quad (3.6)$$

Since the size of the couplings $g_f^{X^n}$ has only a small dependence on n , the largest contributions to the Wilson coefficients come from the effects of the first vector KK excitations, Z_μ^1 and γ_μ^1 . The additional contributions coming from the exchange of the higher KK modes are suppressed by their larger masses and we have checked that our results are negligibly modified by their insertion.

Coefficient	ΔC_9	$\Delta C'_9$	ΔC_{10}	$\Delta C'_{10}$
Best fit value	-1.09	0.46	0.56	-0.25
3σ region	[-1.67, -0.39]	[-0.36, 1.31]	[-0.12, 1.36]	[-0.82, 0.31]

Table 1: *Fitted values for Wilson coefficients from Ref. [6].*

The present experimental results allow to extract a fit of the Wilson coefficients $\Delta C_{9,10}^{(\prime)}$. The ranges of values compatible with the current measurements at the 3σ level are listed in Tab. 1, where the fit includes, on top of the decay $B \rightarrow K^* \mu^+ \mu^-$, observables from $b \rightarrow s \mu^+ \mu^-$, $b \rightarrow s \gamma$ and $b \rightarrow s e^+ e^-$ [6]. The experimental anomalies can be reproduced in our scenario by assuming that the left-handed component of the muon has a sizable degree of compositeness. The right-handed component can instead be almost elementary (for

definiteness we set $c_{\mu_R} = 0.7$). This set-up leaves us with three relevant free parameters which control the localization of the bottom components, $c_{b_{L,R}}$, and that of the μ_L field, c_{μ_L} .

The preferred region in the parameter space is mostly determined by the value of ΔC_9 , which needs to have non-vanishing new-physics contributions in order to fit the experimental results (see Tab. 1). This constraint selects a relatively narrow region in the (c_{b_L}, c_{μ_L}) plane. In particular, at least one of these two parameters is required to be $\lesssim 0.45$, as can be seen from the left panel of Fig. 4. Additional constraints on the (c_{b_L}, c_{μ_L}) plane can be extracted from the bounds on ΔC_{10} . These constraints, however, are quite mild and basically all points compatible with the fit of ΔC_9 are also in agreement with ΔC_{10} .

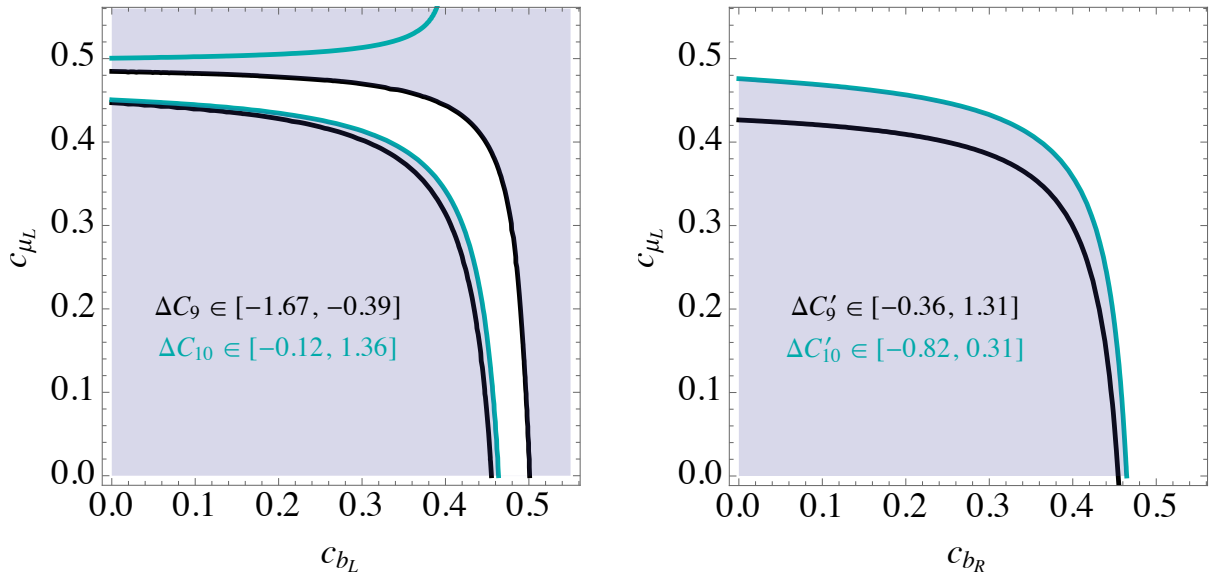


Figure 4: *Left panel: Region in the plane (c_{b_L}, c_{μ_L}) compatible with the fit of ΔC_9 (band between the black solid lines) and ΔC_{10} (band between the green solid lines) at the 3σ level. Right panel: Region in the plane (c_{b_R}, c_{μ_L}) compatible with $\Delta C'_9$ (the region above the black solid line) and $\Delta C'_{10}$ (the region above the blue solid line). In both panels the white region denotes the points allowed by the present data.*

The $\Delta C'_{9,10}$ Wilson coefficients, on the other hand, can be used to select a preferred region in the (c_{b_R}, c_{μ_L}) plane. As can be seen from the right panel of Fig. 4, in this case no strong constraint is found.

4 Constraints

As we discussed in the previous section, the exchange of gauge boson KK modes can give rise to four-fermion interactions that modify the $B \rightarrow K^* \mu^+ \mu^-$ decay. In particular, the anomaly in the current experimental data can be naturally explained in our model provided that the b_L and μ_L fields have a sizable degree of compositeness (i.e. they are localized towards the IR brane). A large compositeness for the light SM fermions, however, also implies that other precision observables can be modified. Noticeable examples are the couplings of the muon and the bottom with the Z -boson and the $\Delta F = 2$ flavor observables. As we will discuss in the following, all these observables are unavoidably linked to the generation of the $\mathcal{O}_{9,10}$ operators and the expected corrections are typically of the same order of the present experimental constraints.

4.1 General overview

As a preliminary step, we find it useful to perform a simple semi-quantitative analysis with the aim of giving an overview of the various new-physics effects that can be used to put bounds on the parameter space of our model. We postpone to the next subsections a detailed discussion and numerical analysis of each experimental constraint.

A first consequence of the large bottom and muon compositeness is the fact that sizable distortions of their couplings with the SM gauge bosons, and in particular with the Z , can be generated. As we mentioned in Sect. 2, after EWSB two effects can induce non-universal distortions of the gauge couplings. The first effect is the mixing of the fermion zero modes with their massive KK towers. The size of these corrections crucially depends on the localization of both the left-handed and the right-handed components of the SM fermions. The second effect comes instead from the mixing between the Z -boson and its vector excitations. In this case the corrections come from diagrams like the one shown in Fig. 5 and the distortion of the coupling for one fermion chirality is independent of the compositeness of the other chirality.

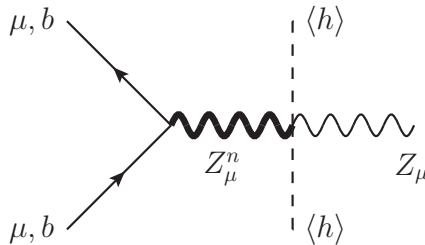


Figure 5: *Feynman diagrams giving rise to the leading contributions to the distortion of the Z couplings to the b -quark and to the muon.*

Since the effects come from the Z -boson mixing and from the fermion KK's are

controlled by different parameters, and are to a large extent independent, they typically do not cancel each other. We can thus use the size of one of them to obtain a lower bound on the overall size of the distortions. In this approximate analysis we will thus only consider the corrections due to the Z mixing, which have a simpler structure and allow to constrain the compositeness of each fermion chirality independently. In the detailed analysis presented in the next subsections we will also take into account the contributions coming from the fermion KK modes.

By using the notation of Eq. (2.17), we can estimate the correction to the SM fermion couplings due to the vector resonances as

$$\frac{\delta g_{Zff}}{g_{Zff}^{SM}} \simeq \sum_n f^{(n)}(c_f) \kappa_n \left(\frac{m_Z}{M_n} \right)^2, \quad (4.1)$$

where κ_n parametrizes the overlap of the Z boson and its n -th KK wave-functions with the Higgs boson. Notice that the κ_n factors are fully determined by the geometry of the extra dimension and by the localization of the Higgs wave-function (or equivalently by the parameter α in the Higgs profile, Eq. (2.9)). Since the κ_n parameters have a small dependence on n , the largest correction to the couplings comes from the mixing of the Z boson with its first KK mode. We can thus approximate the expression in Eq. (4.1) by

$$\frac{\delta g_{Zff}}{g_{Zff}^{SM}} \simeq f^{(1)}(c_f) \kappa_1 \left(\frac{m_Z}{M_1} \right)^2. \quad (4.2)$$

The overlap function $f^{(1)}(c_f)$ is shown in the right panel of Fig. 1. As can be seen from the plot, for values $c_f \lesssim 0.4$ the overlap function can be of order $f^{(1)} \sim \mathcal{O}(\text{few})$, whereas it is suppressed in the region $c_f \gtrsim 0.5$. The second important object in Eq. (4.2) is the κ_1 parameter. For typical values of α which correspond to a natural solution of the hierarchy problem ($\alpha \gtrsim 3$ for the chosen values of the superpotential parameters a and b), one finds $\kappa_1 \gtrsim 1$. Smaller values of κ_1 can be obtained by lowering the value of α (i.e. by pushing the Higgs field towards the UV brane)⁸. In this case, however, an increased amount of tuning is present in the model (see Fig. 2).

The current experimental data put strong bounds on the deviations in the b_L and μ_L couplings to the Z -boson, namely $\delta g_{Zff}/g_{Zff}^{SM} \lesssim \text{few} \times 10^{-3}$. Substituting these constraints into Eq. (4.2), we find

$$|f^{(1)}(c_{f_L})| \simeq \left| \frac{\delta g_{Zf_L f_L}}{g_{Zf_L f_L}^{SM}} \frac{1}{\kappa_1} \right| \left(\frac{M_1}{m_Z} \right)^2 \lesssim 1, \quad f = \mu, b. \quad (4.3)$$

As can be seen from the right panel in Fig. 1, the constraints in Eq. (4.3) roughly correspond to $c_{\mu_L} \gtrsim 0.4$ and $c_{b_L} \gtrsim 0.4$. A comparison with the results of the fit in Fig. 4

⁸In the limit in which the Higgs wave-function becomes flat along the extra dimension, the Higgs VEV does not induce off-diagonal mass terms due to the orthogonality of the KK wave-functions.

shows that the constraints on c_{μ_L} and c_{b_L} must be both saturated in order to allow a large enough contribution to \mathcal{O}_9 .

We can be more quantitative by noticing that the main contribution to ΔC_9 is mediated by the exchange of the first KK modes of the Z -boson and of the photon (see Fig. 3). By using the results in Eqs. (3.3) and (3.5) we find

$$\Delta C_9 \simeq -\frac{\sqrt{2}\pi}{G_{F\alpha}} f^{(1)}(c_{\mu_L}) f^{(1)}(c_{b_L}) \frac{1}{M_1^2} (g_{Zb_L b_L}^{SM} g_{Z\mu_L \mu_L}^{SM} + g_{\gamma b_L b_L}^{SM} g_{\gamma \mu_L \mu_L}^{SM}) \quad (4.4)$$

$$= -\frac{\pi^2 v^2}{s_W^2} \left(1 + \frac{1}{3} \frac{s_W^2}{c_W^2}\right) f^{(1)}(c_{\mu_L}) f^{(1)}(c_{b_L}) \frac{1}{M_1^2}. \quad (4.5)$$

Putting this result together with Eq. (4.2), we finally get

$$\Delta C_9 \simeq -\frac{\pi^2 v^2}{s_W^2} \left(1 + \frac{1}{3} \frac{s_W^2}{c_W^2}\right) \left(\frac{\delta g_{Z\mu_L \mu_L}}{g_{Z\mu_L \mu_L}^{SM}}\right) \left(\frac{\delta g_{Zb_L b_L}}{g_{Zb_L b_L}^{SM}}\right) \frac{1}{\kappa_1^2} \frac{M_1^2}{m_Z^4}. \quad (4.6)$$

The upper value for the contributions to \mathcal{O}_9 can thus be estimated as

$$|\Delta C_9| \lesssim 1, \quad (4.7)$$

which is of the size required to explain the $B \rightarrow K^* \mu^+ \mu^-$ anomaly (see Tab. 1).

A second set of constraints can be derived from $\Delta F = 2$ flavor-changing processes. In the presence of a sizable compositeness for the b_L field, four-fermion contact operators of the form $(\bar{b}_L \gamma^\mu b_L)(\bar{b}_L \gamma_\mu b_L)$ are induced by the exchange of heavy vectors. In particular the largest contributions come from the interactions with the KK modes of the gluons. The KK modes of the Z -boson and of the photon give rise to additional corrections, which are however subleading due to the smaller gauge couplings. As we saw in Sect. 3, after EWSB a mixing among the three quark generations is induced, whose size is parametrized by the CKM matrix elements. Consequently the four-fermion operators involving the b quark give rise to flavor changing contact interactions involving the light-quarks.

Additional four-fermion operators directly involving the light-generation quarks are also typically generated through the exchange of KK vector bosons. These effects are however smaller than the ones coming from the third generation because in our set-up the light quarks have a low amount of compositeness. Moreover, the $U(2)$ flavor structure we assumed for the first two quark generations leads to a further suppression, analogous to the effect discussed in Sect. 3.

The leading contributions to the $\Delta F = 2$ operators involving four left-handed quarks have the form

$$\mathcal{O}_{\Delta F=2}^{LL} \simeq \frac{1}{6} g_s^2 (f^{(1)}(c_{b_L}))^2 \frac{1}{M_1^2} (V_{3i}^* V_{3j})^2 (\bar{d}_{iL} \gamma^\mu d_{jL}) (\bar{d}_{iL} \gamma_\mu d_{jL}), \quad (4.8)$$

where g_s is the QCD gauge coupling and we denoted by d_{iL} ($i = 1, 2, 3$) the down-type left-handed quark in the i -th generation. As can be seen from the above expression, the flavor changing operators follow an approximate MFV structure

$$\mathcal{O}_{\Delta F=2}^{LL} \simeq \mathcal{C}^{LL} (V_{3i}^* V_{3j})^2 (\bar{d}_{iL} \gamma^\mu d_{jL}) (\bar{d}_{iL} \gamma_\mu d_{jL}) . \quad (4.9)$$

The current bounds on the coefficient of the chirality conserving $\Delta F = 2$ operators is of the order $\mathcal{C}^{LL} \lesssim 1/(5 \text{ TeV})^2$ [25, 26] and can be translated into an upper bound on the compositeness of the b_L field, namely

$$|f^{(1)}(c_{b_L})| \lesssim 0.8 . \quad (4.10)$$

This bound is of the same order of the one we derived from the constraints on the Z -boson couplings in Eq. (4.3). This implies that, in order to explain the $B \rightarrow K^* \mu^+ \mu^-$ anomaly, also the corrections to the $\Delta F = 2$ processes are required to be of the order of the present experimental bounds. Similar effects generate also four-fermion $\Delta F = 2$ operators involving right-handed quarks, providing the bound $|f^{(1)}(c_{b_R})| \lesssim 0.8$.

The exchange of vector resonances gives also rise to $\Delta F = 2$ operators involving simultaneously the left- and right-handed quarks. Among these additional operators the most strongly constrained are the ones of the form $(\bar{d}_{iR} d_{jL})(\bar{d}_{iL} d_{jR})$. Analogously to the left-handed operators, we find

$$\mathcal{O}_{\Delta F=2}^{LR} \simeq g_s^2 f^{(1)}(c_{b_L}) f^{(1)}(c_{b_R}) \frac{1}{M_1^2} (V_{3i}^* V_{3j})^2 (\bar{d}_{iR} d_{jL})(\bar{d}_{iL} d_{jR}) . \quad (4.11)$$

In this case, the experimental bounds translate into a combined bound on the amount of compositeness of the left- and right-handed bottom components. As we will discuss in Sect. 4.3, the bounds coming from the LR operators can be more stringent than the LL and RR ones if $c_{b_L} \simeq c_{b_R}$ (see Fig. 11).

Finally, another set of constraints comes from the direct LHC searches for EW vector resonances decaying into a pair of muons and for massive KK gluons decaying into top quarks. In the presence of sizable couplings with the light quarks, the production cross section of the vector boson KK's at the LHC can be significantly high. The current bounds allow to put some constraints on the amount of compositeness of the light quarks and of the bottom.

4.2 Electroweak precision data

In this section we will discuss the main electroweak precision observables which can be used to constrain our model. The most relevant bounds come from the universal oblique observables (encoded by the S , T and U parameters) and from the non-universal correction to the Z coupling with the bottom and the muon.

4.2.1 Oblique corrections

To compare the model predictions with electroweak precision tests (EWPT) we will use the original (S, T, U) variables defined in Ref. [27] (see also Ref. [28]). In our model they are given by the following expressions [12]

$$\begin{aligned}\alpha T &= s_W^2 \frac{m_Z^2}{\rho^2} k^2 y_1 \int_0^{y_1} [1 - \Omega_h(y)]^2 e^{2A(y)-2A_1} dy, \\ \alpha S &= 8c_W^2 s_W^2 \frac{m_Z^2}{\rho^2} k^2 y_1 \int_0^{y_1} \left(1 - \frac{y}{y_1}\right) [1 - \Omega_h(y)] e^{2A(y)-2A_1} dy, \\ \alpha U &\simeq 0,\end{aligned}\tag{4.12}$$

where $\rho = ke^{-A(y_1)}$ and

$$\Omega_h(y) = \frac{\omega(y)}{\omega(y_1)}, \quad \omega(y) = \int_0^y h^2(\bar{y}) e^{-2A(\bar{y})} d\bar{y}.\tag{4.13}$$

These expressions include the leading contributions, which are due to the tree-level mixing of the SM gauge bosons with the massive vector KK modes. The present experimental

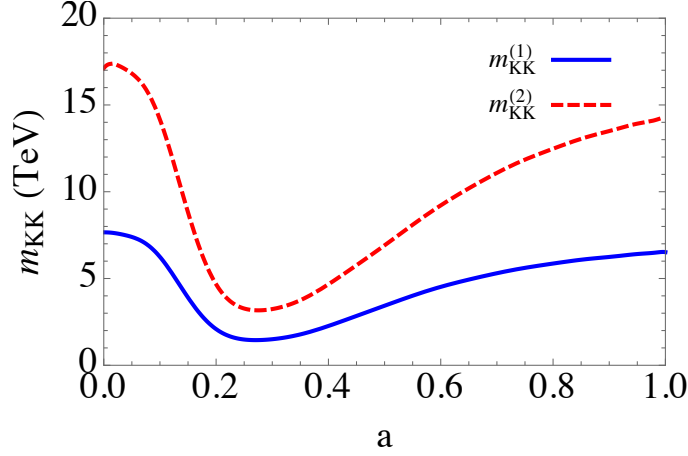


Figure 6: *Bounds on m_{KK} in TeV, as a function of a , for $b = 1$, from oblique observables.*

bounds on the S and T parameter are given by [29]

$$T = 0.05 \pm 0.07, \quad S = 0.00 \pm 0.08 \quad (90\% \text{ correlation}).\tag{4.14}$$

These constraints imply a lower bound on the mass of the vector KK modes. The bounds on m_{KK} as a function of a are shown in Fig. 6 (for the choice $b = 1$). For different values of b a similar behavior of the bounds is obtained.

As can be seen from the plot in Fig. 6, for $a \sim 0.25$ a significant reduction in the bound is present. In particular for the value of the parameters chosen in this paper, $b = 1$ and $a = 0.2$, the bound on the mass of the first KK mode is $m_{KK} \gtrsim 2$ TeV. The reduction in the bounds is one of the peculiar features of soft-wall metrics, as the one we are using in our model. Even in the absence of a custodial symmetry in the bulk, the contributions to the oblique parameters are suppressed if the soft wall singularity is not far away from the IR brane. One way of understanding this effect is to look at the shape of the normalized physical Higgs wave function in the presence of the soft-wall metric (\tilde{h}_{SW}) [15, 17]

$$\tilde{h}_{SW}(y) = \frac{\sqrt{y_1}}{\sqrt{\int e^{-2A+2\alpha ky}}} e^{-A+\alpha ky} \quad (4.15)$$

It turns out that there is a local maximum of the function \tilde{h}_{SW} for values of $y < y_1$, unlike in the pure RS case in which \tilde{h}_{RS} grows monotonically from the UV to the IR brane. As a consequence $\tilde{h}_{SW}(y_1) < \tilde{h}_{RS}(y_1)$ and, since the KK-modes are localized towards the IR brane, there is a significant reduction in the EWSB-induced mass mixing with the gauge zero modes. This results in a suppression of the corrections to the S and T observables with respect to the RS scenario.

4.2.2 The $Z\bar{b}b$ coupling

As we mentioned in the general discussion in Sect. 4.1, the Z boson couplings to SM fermions with a sizable degree of compositeness can be modified by two independent effects: one coming from the vector KK modes and the other from the fermion KK excitations. The diagrams induced by these two effects in the case of the $Z_\mu \bar{b}_{L,R} \gamma^\mu b_{L,R}$ couplings are shown in Fig. 7. The distortion in the couplings can be straightforwardly

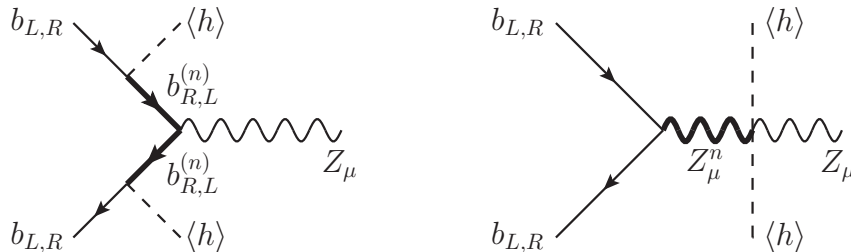


Figure 7: Feynman diagrams contributing to the coupling $Z\bar{b}b$.

written as a sum over the contributions of the various KK modes, as we did to derive the approximate result in Eq. (4.1). It is however possible to carry out explicitly the sum over the KK levels, thus obtaining the full result [16]

$$\delta g_{b_{L,R}} = -g_{b_{L,R}}^{SM} m_Z^2 \hat{\alpha}_{b_{L,R}} \pm g \frac{v^2}{2} \hat{\beta}_{b_{L,R}}, \quad (4.16)$$

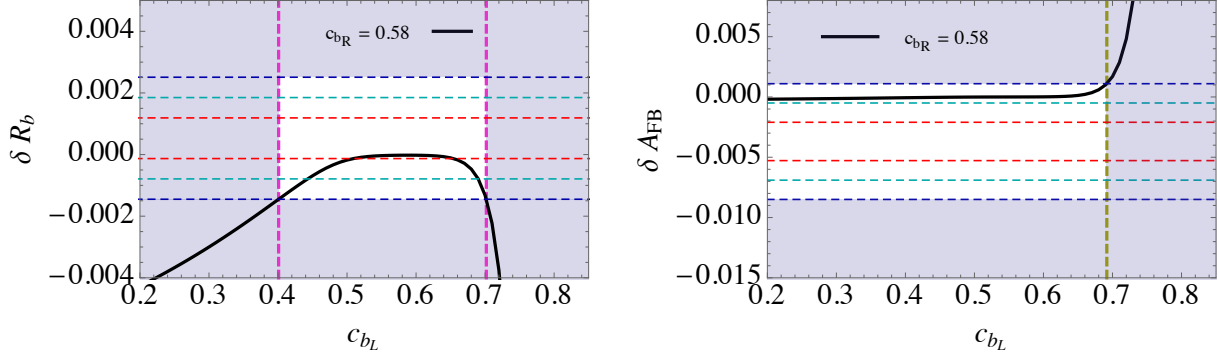


Figure 8: Value of δR_b (left panel) and δA_{FB} (right panel) as a function of c_{b_L} obtained in a scenario with no tuning in the Higgs sector ($\alpha = 3$). In both panels we fixed $c_{b_R} = 0.58$ (other values of c_{b_R} do not lead to significant changes). The horizontal lines in both figures correspond to the experimental bounds at 1σ , 2σ and 3σ .

where $g_{b_{L,R}}^{SM}$ denote the (tree-level) Z coupling to the $b_{L,R}$ fields in the SM, while

$$\begin{aligned}\widehat{\alpha}_{b_{L,R}} &= y_1 \int_0^{y_1} e^{2A} \left(\Omega_h - \frac{y}{y_1} \right) (\Omega_{b_{L,R}} - 1) , \\ \widehat{\beta}_{b_{L,R}} &= y_b^2 \int_0^{y_1} e^{2A} \left(\frac{d\Omega_{b_{R,L}}}{dy} \right)^{-1} (\Gamma_b - \Omega_{b_{R,L}})^2 ,\end{aligned}\quad (4.17)$$

with y_b the bottom quark Yukawa coupling and

$$\Omega_{b_{L,R}} = \frac{\int_0^y e^{(1-2c_{b_{L,R}})A}}{\int_0^{y_1} e^{(1-2c_{b_{L,R}})A}}, \quad \Gamma_b = \frac{\int_0^y h e^{-(c_{b_L} + c_{b_R})A}}{\int_0^{y_1} h e^{-(c_{b_L} + c_{b_R})A}}. \quad (4.18)$$

It is easy to recognize that the two terms in Eq. (4.16) correspond respectively to the effects of the massive vectors and of the fermion KK modes ⁹.

The experimental constraints on the $Z\bar{b}b$ coupling come from the Z -pole observables measured at LEP, in particular R_b , the ratio of the $Z \rightarrow \bar{b}b$ partial width to the inclusive hadronic width, and A_{FB}^b , the forward-backward asymmetry of the bottom quark. In addition SLD directly measured the bottom asymmetry A_b with longitudinal beam polarizations. These three quantities are related at tree-level to the $Z\bar{b}b$ couplings by

$$R_b = \frac{g_{b_L}^2 + g_{b_R}^2}{g_{b_L}^2 + g_{b_R}^2 + \sum_{q \neq t,b} (g_{q_L}^2 + g_{q_R}^2)}, \quad A_b = \frac{g_{b_L}^2 - g_{b_R}^2}{g_{b_L}^2 + g_{b_R}^2}, \quad A_{FB}^b = \frac{3g_{e_L}^2 - g_{e_R}^2}{4g_{e_L}^2 + e_{b_R}^2} A_b. \quad (4.19)$$

⁹In our computation we are not including additional contributions coming from the mixing of the bottom quark with the light-generations quarks that is induced after EWSB. This effect is however negligible since the mixing matrix is highly hierarchical.

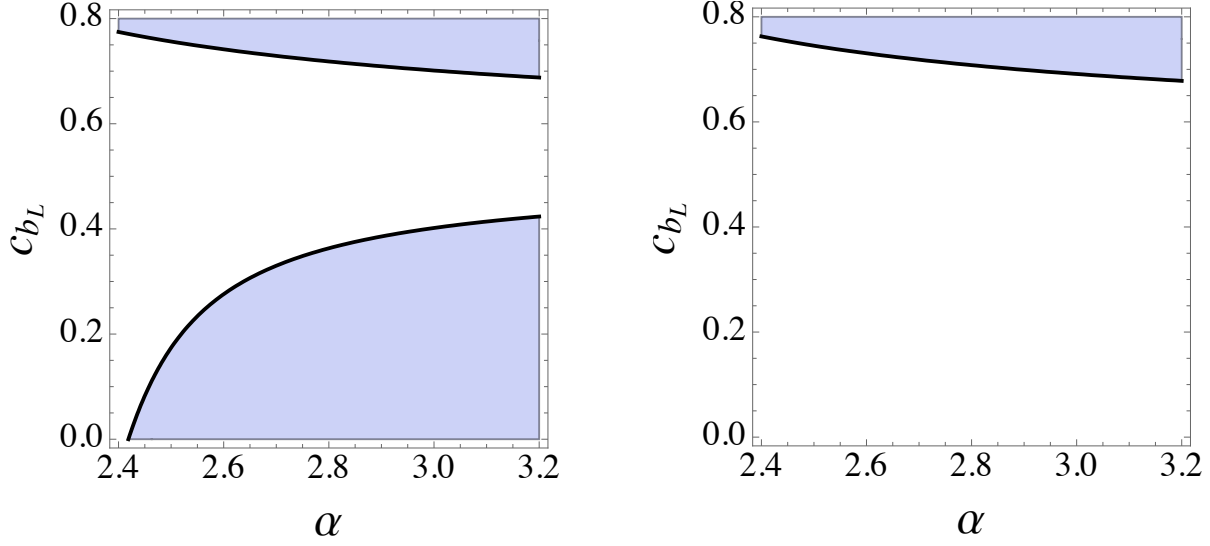


Figure 9: Region in the plane (α, c_{b_L}) allowed (unshaded area) by experimental data on δR_b (left panel) and δA_{FB}^b (right panel) at the 3σ level. In both panels we have fixed $c_{b_R} = 0.58$ (other values of c_{b_R} do not lead to significant changes).

From these expressions we can extract the contributions induced by the coupling modifications

$$\begin{aligned}
\delta R_b &= -0.606 \delta g_{b_L} + 0.110 \delta g_{b_R}, \\
\delta A_b &= -0.227 \delta g_{b_L} - 1.25 \delta g_{b_R}, \\
\delta A_{FB}^b &= -0.026 \delta g_{b_L} - 0.141 \delta g_{b_R}.
\end{aligned}
\tag{4.20}$$

The experimental values for the above observables are given by [29]

$$\begin{aligned}
\delta R_b^{exp} &= 0.00053 \pm 0.00066, \\
\delta A_b^{exp} &= -0.0117 \pm 0.020, \\
\delta A_{FB}^{b,exp} &= -0.0037 \pm 0.0016.
\end{aligned}
\tag{4.21}$$

The values of δR_b and δA_{FB} as functions of c_{b_L} are plotted in Fig. 8 (for $c_{b_R} = 0.58$). To derive these results we chose $\alpha = 3$, which corresponds to a completely Natural scenario with no tuning in the Higgs sector. One can see that already in the SM ($\delta R_b = \delta A_{FB} = 0$) some tension slightly above the 2σ level is present in the data. In our model we are never able to reduce the tension, although for a sizable range of the parameters the agreement with the data is the same as in the SM. We extract a constraint on c_{b_L} by allowing only configurations which agree with the data within the 3σ range. In this way we find $0.4 \lesssim c_{b_L} \lesssim 0.7$.

If some amount of tuning is allowed in the Higgs sector (i.e. for $\alpha < 3$), the Higgs background wave-function becomes more flat and the EWSB mixing among different KK

levels decreases. In this case the corrections to the Z couplings can be reduced and the bounds on the b compositeness relaxed. We show in Fig. 9 how the bounds on $c_{b_{L,R}}$ vary as a function of α . The amount of fine tuning as a function of α was plotted in Fig. 2. If we allow for a 5% tuning (corresponding to $\alpha \simeq 2.9$), the bounds are slightly relaxed to $0.37 \lesssim c_{b_L} \lesssim 0.71$. Notice however that the tuning increases exponentially for $\alpha \lesssim 2.95$, thus a further significant reduction of the bounds would require unacceptably high tuning.

4.2.3 The $Z\bar{\mu}\mu$ coupling

Analogously to the bottom couplings to the Z , the massive KK modes also induce modifications of the muon couplings. The explicit formulae for these corrections can be obtained from Eqs. (4.16), (4.17) and (4.18) with obvious substitutions.

The current bounds on the distortions of the muon couplings to the Z are given in Ref. [29]. In our scenario we assumed that the right-handed muon component is almost elementary, thus its coupling does not deviate appreciably from its SM value, $\delta g_{\mu_R}(c_{\mu_R}) \simeq 0$. In this case the bounds on the deviation of the μ_L coupling are given by $|\delta g_{\mu_L}(c_{\mu_L})/g_{\mu_L}^{SM}| \lesssim 5 \times 10^{-3}$ at 95% CL.

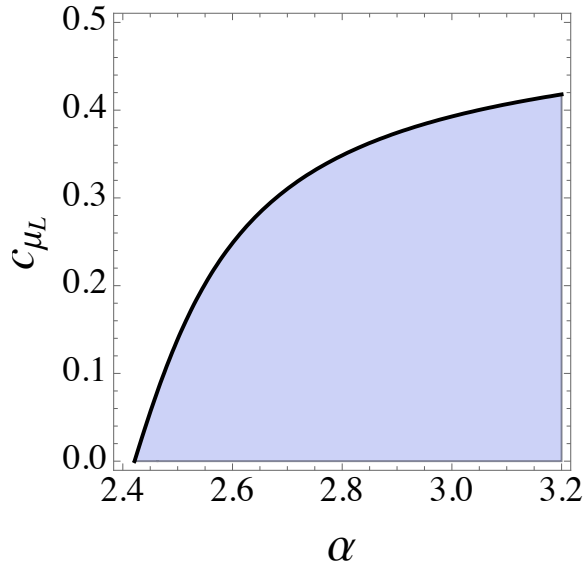


Figure 10: Region in the plane (α, c_{μ_L}) with the contour line $\delta g_{\mu_L,R}^Z(c_{\mu_L,R})/g_{\mu_L,R}^{Z,SM} \leq 5 \times 10^{-3}$.

As in the case of the bottom coupling, also the μ_L coupling to the Z depends on the amount of compositeness of the fermion as well as on the localization of the Higgs, i.e. by the parameter α . Smaller values of α imply a reduction of the corrections, at the price of an increased amount of tuning in the Higgs sector. The bound on c_{μ_L} as a function of α is shown in Fig. 10. Requiring our model to be completely Natural implies the constraint $c_{\mu_L} \gtrsim 0.4$. If we accept a tuning of the order of 5% the constraint is relaxed to $c_{\mu_L} \gtrsim 0.37$.

4.3 Flavor observables

Another important set of constraints comes from $\Delta F = 2$ flavor-changing processes mediated by four-fermion contact interactions. These observables can be used to put some bounds on the amount of compositeness of the bottom quark.

As we already discussed in Sect. 4.1, the main new-physics contributions to $\Delta F = 2$ processes come from the exchange of gluon KK modes. The leading flavor-violating couplings of the KK gluons involving the down-type quarks are given by (compare with Eq. (3.4))

$$\mathcal{L}_s = G_{n\mu}^A \left[V_{3i}^* V_{3j} \bar{d}_i \gamma^\mu \{ (g_{b_L}^{G^n} - \bar{g}_L^{G^n}) P_L + (g_{b_R}^{G^n} - \bar{g}_R^{G^n}) P_R \} d_j + \text{h.c.} \right], \quad (4.22)$$

where the $g_{f_{L,R}}^{G^n}$ couplings are given by

$$g_{f_{L,R}}^{G^n} = g_s f^{(n)}(c_{f_{L,R}}). \quad (4.23)$$

In Eq. (4.22), $\bar{g}_{L,R}^{G^n}$ denote the KK-gluon couplings to the first and second generation down quarks, which are universal due to the $U(2)$ flavor symmetry present in our model, namely $\bar{g}_{L,R}^{G^n} = \bar{g}_{d_{1L,R}}^{G^n} = \bar{g}_{d_{2L,R}}^{G^n}$.

After integrating out the massive KK gluons, the couplings in Eq. (4.22) give rise to the following set of $\Delta F = 2$ dimension-six operators

$$\begin{aligned} \mathcal{L}_{\Delta F=2} = \sum_n \left\{ \frac{c_{ij}^{LL(n)}}{M_n^2} (\bar{d}_{iL} \gamma^\mu d_{jL}) (\bar{d}_{iL} \gamma_\mu d_{jL}) + \frac{c_{ij}^{RR(n)}}{M_n^2} (\bar{d}_{iR} \gamma^\mu d_{jR}) (\bar{d}_{iR} \gamma_\mu d_{jR}) \right. \\ \left. + \frac{c_{ij}^{LR(n)}}{M_n^2} (\bar{d}_{iR} d_{jL}) (\bar{d}_{iL} d_{jR}) \right\}, \end{aligned} \quad (4.24)$$

where

$$\begin{aligned} c_{ij}^{LL,RR(n)} &= \frac{1}{6} (V_{3i}^* V_{3j})^2 (g_{b_{L,R}}^{G^n} - \bar{g}_{L,R}^{G^n})^2, \\ c_{ij}^{LR(n)} &= (V_{3i}^* V_{3j})^2 (g_{b_L}^{G^n} - \bar{g}_L^{G^n}) (g_{b_R}^{G^n} - \bar{g}_R^{G^n}). \end{aligned} \quad (4.25)$$

The current bounds on the $\Delta F = 2$ contact operators [25, 26] can be translated into constraints on the quantities

$$\sum_n \frac{(g_{b_{L,R}}^{G^n} - \bar{g}_{L,R}^{G^n})^2}{M_n^2 [\text{TeV}]} \simeq \sum_n \frac{(g_{b_{L,R}}^{G^n})^2}{M_n^2 [\text{TeV}]} \leq 0.14, \quad (4.26)$$

$$\sum_n \frac{(g_{b_L}^{G^n} - \bar{g}_L^{G^n}) (g_{b_R}^{G^n} - \bar{g}_R^{G^n})}{M_n^2 [\text{TeV}]} \simeq \sum_n \frac{g_{b_L}^{G^n} g_{b_R}^{G^n}}{M_n^2 [\text{TeV}]} \leq 3 \times 10^{-4}, \quad (4.27)$$

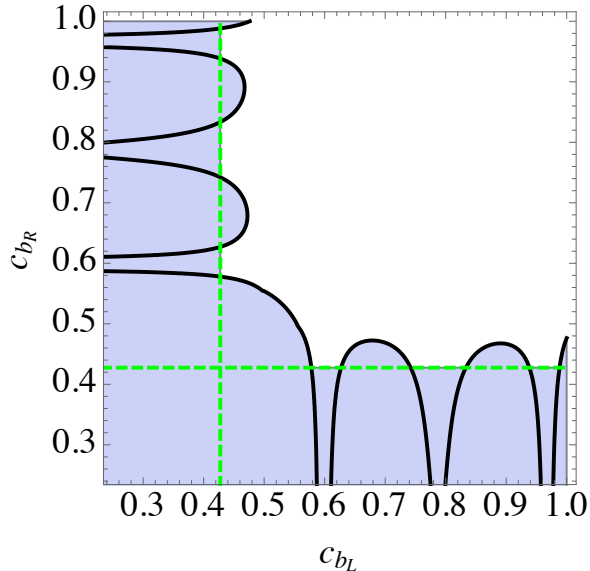


Figure 11: *Region in the plane (c_{b_L}, c_{b_R}) that accommodates the bound of Eqs. (4.26) and (4.27). The dashed green lines represent the constraints in Eq. (4.28). The allowed points correspond to the unshaded region.*

where, to simplify the full expressions, we used the fact that $\bar{g}_{L,R}^{G^n} \ll g_{b_{L,R}}^{G^n}$ which follows from our assumption that the light-generation quarks are almost elementary.

The bound in Eq. (4.26) is quite interesting since it allows to derive independent constraints on the amount of compositeness of the b_L and b_R components or, in other words, on the c_{b_L} and c_{b_R} parameters. At the 95% CL we find

$$c_{b_{L,R}} \geq 0.43. \quad (4.28)$$

The constraint in Eq. (4.27) gives instead a combined bound on the b_L and b_R compositeness. The allowed configurations in the (c_{b_L}, c_{b_R}) plane are shown in Fig. 11. One can see that the bound from the LR operators dominates for $c_{b_L} \simeq c_{b_R} \simeq 0.5$, whereas if only one bottom chirality has a sizable compositeness, the bounds from LL, RR and LR operators are of the same order.

4.4 The ATLAS di-muon resonance search

An additional experimental constraint comes from direct searches for high-mass resonances decaying into di-muon final states. This search has been performed by the ATLAS Collaboration both at $\sqrt{s} = 8$ TeV with an integrated luminosity of 20.3 fb^{-1} [30], and at $\sqrt{s} = 13$ TeV with an integrated luminosity of 3.2 fb^{-1} [31].

In our model this search can be sensitive to the production of the massive excitations of the Z and of the photon. The resonances Z_μ^n and γ_μ^n can be produced by Drell-Yan

processes and decay into a pair of leptons as shown in the diagram of Fig. 12. The decay

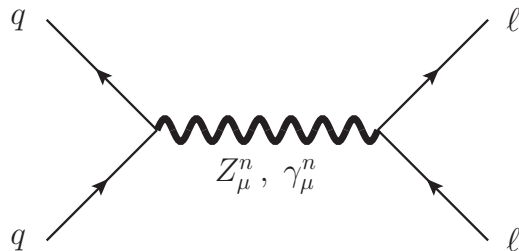


Figure 12: *Drell-Yan contribution to the process $\sigma(pp \rightarrow X_n \rightarrow \ell\ell)$.*

width of X^n ($X = Z, \gamma$) into a fermion pair $f\bar{f}$ is given at the tree-level by

$$\Gamma(X_n \rightarrow f\bar{f}) = N_c M_n \frac{\sqrt{2} G_F m_Z^2}{24\pi g^2} \left[(g_{f_L}^{X_n})^2 + (g_{f_R}^{X_n})^2 \right], \quad (4.29)$$

where $N_c = 3$ (1) for quarks (leptons) and we neglected the effect of fermion masses. In the narrow width approximation (NWA) the cross-section for the process $pp \rightarrow Z^n/\gamma^n \rightarrow \mu^+\mu^-$ approximately scales as

$$\sigma(pp \rightarrow Z_n/\gamma_n \rightarrow \mu^+\mu^-) \propto A = \sum_{X=Z,\gamma} A_{X^n},$$

$$A_{X^n} = \frac{g_{\mu_L}^2 (2g_{u_L}^2 + 2g_{u_R}^2 + g_{d_L}^2 + g_{d_R}^2)}{3(g_{b_L}^2 + g_{t_L}^2 + g_{b_R}^2 + g_{t_R}^2) + \sum_{\ell=\mu,\tau} (g_{\ell_L}^2 + g_{\nu_\ell}^2 + g_{\ell_R}^2)}, \quad (4.30)$$

where all couplings refer to the $g_{f_{L,R}}^{X^n}$ couplings and for simplicity we have omitted the superscript X^n . To obtain the above formula we neglected, in the denominator of Eq. (4.30), the contributions from the light quarks (u, d, s, c) and leptons (e, ν_e) to the decay width.

The 13 TeV ATLAS experimental bound [31], translates into the constraint $A < 0.022$ ($A < 0.003$) for $M_n = 3$ TeV ($M_n = 2$ TeV) at 95% CL. To get an idea of the bounds on the parameter space of our model we reduce the number of free parameters by setting a common value for the compositeness of the light quarks $c_{q_L} = c_{q_R} \equiv c_q$ for $q = u, d$. The constraints in the plane (c_q, c_{μ_L}) are shown in Fig. 13, for a benchmark choice of the parameters. The numerical results show that for almost elementary light quarks $c_q \gtrsim 0.46$ basically no bound is present on the amount of μ_L compositeness.

4.5 Direct searches on KK gluons

A second set of direct constraints comes from searches of massive gluon KK modes. Since the gluons are the most strongly coupled KK modes, they should be more copiously

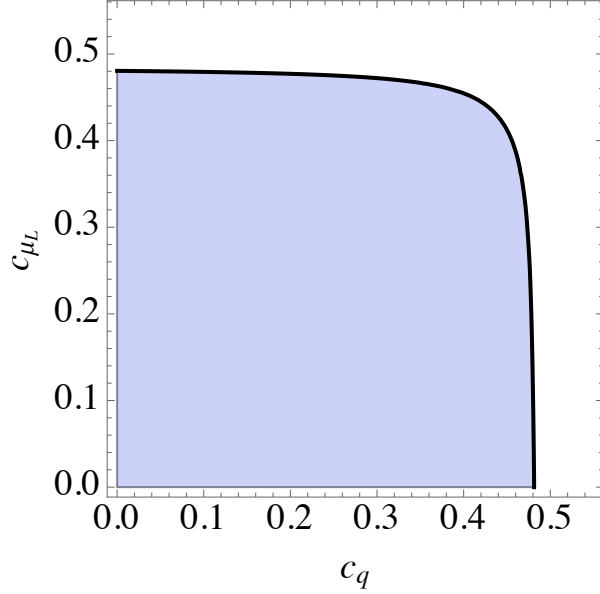


Figure 13: *Exclusions in the plane (c_q, c_{μ_L}) coming from the searches of massive resonances decaying into di-muons. The results are derived for the following benchmark choice of the parameters: $c_{\mu_R} = 0.7$, $c_{\tau_R} = 0.6$, $c_{b_R} = 0.6$, $c_{t_R} = -0.5$, $c_{b_L} = 0.43$, $c_{\tau_L} = c_{\mu_L}$. The remaining parameters have been fixed by requiring the quark masses to be reproduced for values of the Yukawa couplings $\sqrt{k\hat{Y}} = 3$.*

produced than EW KK modes and easily detected at the LHC due to the sizable branching ratio into $\bar{t}t$. On the other hand, since the EWSB contribution to the mass of the KK modes is negligible, it turns out, as was already noticed, that all gauge boson KK modes are approximately degenerate in mass. Therefore the bounds on the mass of gluon KK modes directly translates into bounds on the mass M_n of all vector KK modes.

Direct searches for KK gluons G_{μ}^n , in the RS scenarios, have been performed by CMS [32], for an integrated luminosity of 19.7 fb^{-1} and $\sqrt{s} = 8 \text{ TeV}$, and by ATLAS [33], for an integrated luminosity of 20.3 fb^{-1} and $\sqrt{s} = 8 \text{ TeV}$, by measuring the cross-section $\sigma(pp \rightarrow \bar{t}t)$. The KK gluon is produced by the DY mechanism from light quarks and decays preferentially into top quarks. The experimental searches focus on the lepton plus jets final state, where the top pair decays into $W^+bW^- \bar{b}$, one W decaying leptonically and the other hadronically. The 95% CL bounds obtained in these searches are

$$M_1^{RS} \gtrsim 2.5 \text{ TeV (CMS)}, \quad M_1^{RS} \gtrsim 2.2 \text{ TeV (ATLAS)}. \quad (4.31)$$

These bounds are derived in a RS set-up with light fermions localized towards the UV brane ($c_f > 0.5$) whose coupling to the first KK gluon excitation has the value $g_{G_{RS}^1 \bar{f}f} \simeq 0.2 g_s$ [34]. In our model, instead, this coupling is significantly smaller, $g_{G^1 \bar{f}f} \simeq 0.13 g_s$ (see Fig. 1). This translates into a slightly weaker bound, namely $M_1 \gtrsim 2 \text{ TeV}$, which coincides with our benchmark choice for the KK scale. We want to stress here that our

choice of $M_1 \simeq 2$ TeV is just a benchmark point and the results found in our analysis would be essentially unchanged by slightly increasing this value.

5 Conclusions

In this paper we explored a modified RS model as a possible explanation of the recently-found anomalies in the semi-leptonic B -meson decays. The attractiveness of our scenario is the fact that the new dynamics that generates the flavor anomalies is *not ad-hoc*, but instead is intrinsically linked to the mechanism that in RS scenarios ensures a natural solution of the EW Hierarchy Problem. The corrections to the B -meson physics are indeed due to $\Delta F = 1$ four-fermion contact interactions induced by the exchange of the heavy KK modes of the Z -gauge boson and of the photon. These modes are unavoidably present in the RS scenarios in which the SM gauge invariance is also extended into the bulk.

Sizable corrections to the $\Delta F = 1$ processes can be obtained provided that the left-handed components of the bottom quark and of the muon lepton have a sizable degree of compositeness, i.e. that they are sufficiently localized towards the IR brane. In this case large couplings to the gauge KK modes are generated, which translate into sizable contributions to the contact operators $\mathcal{O}_{9,10}$. Additional contributions to operators involving the right-handed quarks $\mathcal{O}'_{9,10}$ could also be generated if the b_R quark is sufficiently IR localized.

The main quantities that control the $\Delta F = 1$ effects are thus the 5D bulk masses of the bottom and the muon fields, which are conveniently encoded in the $c_{b_{L,R}}$ and c_{μ_L} parameters. The parameter space region that allows to fit the current flavor anomalies is shown in Fig. 4. The strongest constraints on the parameter space of our model come from the requirement of inducing a large enough contribution to the \mathcal{O}_9 operator (see Tab. 1). This implies that at least one of the conditions $c_{\mu_L} \lesssim 0.45$ and $c_{b_L} \lesssim 0.45$ must be satisfied. The b_R field can instead be almost elementary ($c_{b_R} \gtrsim 0.5$).

As a consequence of the large amount of compositeness for the μ_L and/or b_L fields, sizable corrections in the electroweak and flavor observables can be generated. Deviations in the $g_{Z\bar{\mu}\mu}$ and $g_{Z\bar{b}b}$ couplings are indeed expected and can be used to put some bounds on c_{μ_L} and c_{b_L} . In a completely Natural model one finds $c_{\mu_L} \gtrsim 0.4$ and $c_{b_L} \gtrsim 0.4$. These bounds can be slightly relaxed, at the price of introducing some fine-tuning in the Higgs mass, by modifying the localization of the Higgs field. A fine-tuning of the order of 5% allows to weaken the bounds to $c_{\mu_L}, c_{b_L} \gtrsim 0.37$ (see Figs. 8 and 10). Notice however that the amount of tuning increases exponentially when one tries to further lower these bounds, thus quickly reaching unacceptably high values.

Even stronger bounds can be derived from flavor observables, most noticeably $\Delta F = 2$ processes. The exchange of massive vector fields (in particular the KK modes of the

gluons) gives rise to four-fermion contact interactions involving the SM quarks. After EWSB these operators can develop flavor-changing components due to the mixing among the various generations induced by the Yukawa couplings. Contact operators involving the down-type quarks are fully controlled by the amount of compositeness of the b_L and b_R fields and by the CKM matrix elements. The flavor data can thus be directly translated into bounds $c_{b_L} \gtrsim 0.43$, and $c_{b_R} \gtrsim 0.43$ which can not be evaded in our set-up. Even stronger bounds are found for $c_{b_L} \simeq c_{b_R}$, in which case $c_{b_{L,R}} \gtrsim 0.5$ (see Fig. 11).

Finally additional constraints on the amount of compositeness of the first generation quarks can be derived from the LHC searches for resonances decaying into a muon pair, as well as from direct searches of KK gluons. These constraints are however easily fulfilled in our model by assuming that the first generation quarks are localized toward the UV and thus weakly coupled to the gauge KK modes (see Fig. 13).

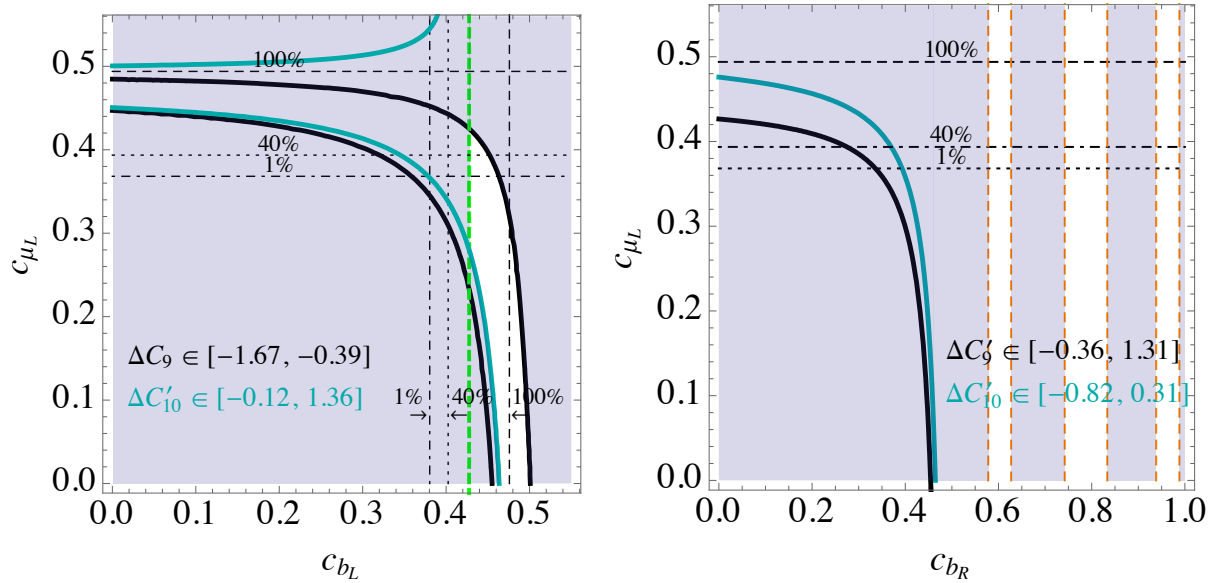


Figure 14: *Left panel: Region in the plane (c_{b_L}, c_{μ_L}) that accommodates ΔC_9 (the band inside the black solid lines) and $\Delta C'_{10}$ (the band inside the green solid lines). The points to the left of the vertical dashed green line are excluded by the flavor bound in Eq. (4.27). The fine-tuning needed to pass the constraints on the modification of the $Z\mu\bar{\mu}$ ($Z\bar{b}b$) coupling is shown by the black dashed, dotted and dot-dashed horizontal (vertical) lines (see Sects. 4.2.3 and 4.2.2). Right panel: Region in the plane (c_{b_R}, c_{μ_L}) that accommodates $\Delta C'_9$ (the region outside the black solid line) and $\Delta C'_{10}$ (the region outside the blue solid line) for the benchmark choice $c_{b_L} = 0.43$. The allowed white bands are determined by the flavor constraints.*

The results of our analysis are summarized in Fig. 14, where we show the parameter space regions in the (c_{b_L}, c_{μ_L}) and (c_{b_R}, c_{μ_L}) planes that allow to fit the flavor anomalies, together with the constraints coming from EW and flavor precision measurements. The regions allowed by all constraints correspond to the un-shadowed areas. Notice that in the

plots we did not include the lower bound for c_{μ_L} implied by the corrections to the $Z\bar{\mu}_L\mu_L$ vertex. We instead showed the amount of fine tuning in the Higgs sector that is needed to pass the EW constraints for each value of c_{μ_L} . The dashed horizontal line corresponds to a completely Natural scenario, whereas the dotted and dot-dashed lines correspond respectively to 40% and 1% tuning. Analogously, the constraints from the corrections to the $Z\bar{b}b$ couplings (in particular the observables δA_b and δA_{FB}^b) corresponding to a certain level of tuning are shown by the dashed, dotted and dot-dashed vertical lines in the left plot. These constraints are however weaker than the one derived from flavor observables, $c_{b_L} > 0.43$ (shown by the dashed green line in the plot).

To obtain the plot in the right panel we fixed $c_{b_L} = 0.43$, the minimum value allowed by $\Delta F = 2$ flavor constraints. For larger value of c_{b_L} , i.e. $c_{b_L} \gtrsim 0.45$, the allowed region in the right panel plot would be $c_{b_R} \gtrsim 0.55$ as one can infer from Fig. 11.

An interesting outcome of our analysis is the fact that, in a completely Natural model with no tuning in the Higgs sector, requiring the flavor anomalies to be reproduced almost completely fix the values of the parameters $c_{b_L} \simeq c_{\mu_L} \simeq 0.45$. In this configuration the corrections to the $\Delta F = 2$ observables and the deviations in the Z couplings to the b_L and μ_L fields are all expected to be close to the present experimental bounds. This is a quite sharp prediction of our scenario, which predicts correlated deviations potentially testable in not so far future experiments.

Finally, let us also add that the concrete model studied here also sharply predicts the presence of a dilaton-like scalar with mass around 100 GeV, see Ref. [18]. As discussed in Refs. [35–38] such a light dilaton can appear naturally in this kind of models, and it is experimentally allowed basically because its couplings to SM fields are slightly suppressed [18, 19]. This dilaton-like state looks quite unrelated to the flavor physics and there might be other extra-dimensional models that manage to address the flavor anomalies and Naturalness without it. In the class of models analyzed here, its presence is related to the fact that the model passes all tests with a low KK scale ~ 2 TeV.

ACKNOWLEDGMENTS

The work of G.P., O.P. and M.Q. is partly supported by MINECO under Grant CICYT-FEDER-FPA2014-55613-P, by the Severo Ochoa Excellence Program of MINECO under the grant SO-2012-0234 and by Secretaria d'Universitats i Recerca del Departament d'Economia i Coneixement de la Generalitat de Catalunya under Grant 2014 SGR 1450. E.M. would like to thank the Institut de Física d'Altes Energies (IFAE), Barcelona, Spain, and the Instituto de Física Teórica CSIC/UAM, Madrid, Spain, for their hospitality during the completion of the final stages of this work. The work of E.M. is supported by the European Union under a Marie Curie Intra-European Fellowship (FP7-PEOPLE-2013-IEF) with project number PIEF-GA-2013-623006.

References

- [1] R. Aaij *et al.* [LHCb Collaboration], Phys. Rev. Lett. **113** (2014) 151601 [[arXiv:1406.6482](#) [hep-ex]].
- [2] R. Aaij *et al.* [LHCb Collaboration], JHEP **1602** (2016) 104 [[arXiv:1512.04442](#) [hep-ex]].
- [3] A. Abdesselam *et al.* [Belle Collaboration], [arXiv:1604.04042](#) [hep-ex].
- [4] S. Descotes-Genon, J. Matias and J. Virto, Phys. Rev. D **88**, 074002 (2013) doi:10.1103/PhysRevD.88.074002 [[arXiv:1307.5683](#) [hep-ph]]; W. Altmannshofer and D. M. Straub, Eur. Phys. J. C **73** (2013) 2646 [[arXiv:1308.1501](#) [hep-ph]]; R. Gauld, F. Goertz and U. Haisch, Phys. Rev. D **89** (2014) 015005 [[arXiv:1308.1959](#) [hep-ph]]; W. Altmannshofer, S. Gori, M. Pospelov and I. Yavin, Phys. Rev. D **89** (2014) 095033 [[arXiv:1403.1269](#) [hep-ph]]; A. Crivellin, G. D'Ambrosio and J. Heeck, Phys. Rev. Lett. **114**, 151801 (2015) [[arXiv:1501.00993](#) [hep-ph]]; D. Aristizabal Sierra, F. Staub and A. Vicente, Phys. Rev. D **92** (2015) no.1, 015001 [[arXiv:1503.06077](#) [hep-ph]]; A. Crivellin, L. Hofer, J. Matias, U. Nierste, S. Pokorski and J. Rosiek, Phys. Rev. D **92** (2015) no.5, 054013 [[arXiv:1504.07928](#) [hep-ph]]; A. Celis, J. Fuentes-Martin, M. Jung and H. Serodio, Phys. Rev. D **92** (2015) no.1, 015007 [[arXiv:1505.03079](#) [hep-ph]]; W. Altmannshofer and I. Yavin, Phys. Rev. D **92** (2015) no.7, 075022 [[arXiv:1508.07009](#) [hep-ph]]; A. Falkowski, M. Nardecchia and R. Ziegler, JHEP **1511** (2015) 173 [[arXiv:1509.01249](#) [hep-ph]]; S. Descotes-Genon, L. Hofer, J. Matias and J. Virto, JHEP **1606** (2016) 092 [[arXiv:1510.04239](#) [hep-ph]]; B. Allanach, F. S. Queiroz, A. Strumia and S. Sun, Phys. Rev. D **93** (2016) no.5, 055045 [[arXiv:1511.07447](#) [hep-ph]]; S. M. Boucenna, A. Celis, J. Fuentes-Martin, A. Vicente and J. Virto, Phys. Lett. B **760**, 214 (2016) doi:10.1016/j.physletb.2016.06.067 [[arXiv:1604.03088](#) [hep-ph]]; D. Buttazzo, A. Greljo, G. Isidori and D. Marzocca, [arXiv:1604.03940](#) [hep-ph]; S. M. Boucenna, A. Celis, J. Fuentes-Martin, A. Vicente and J. Virto, JHEP **1612**, 059 (2016) doi:10.1007/JHEP12(2016)059 [[arXiv:1608.01349](#) [hep-ph]].
- [5] C. Niehoff, P. Stangl and D. M. Straub, Phys. Lett. B **747** (2015) 182 [[arXiv:1503.03865](#) [hep-ph]].
- [6] S. Descotes-Genon, L. Hofer, J. Matias and J. Virto, JHEP **1606**, 092 (2016) doi:10.1007/JHEP06(2016)092 [[arXiv:1510.04239](#) [hep-ph]]; S. Descotes-Genon, L. Hofer, J. Matias and J. Virto, [arXiv:1605.06059](#) [hep-ph].
- [7] N. Kosnik, Phys. Rev. D **86** (2012) 055004 [[arXiv:1206.2970](#) [hep-ph]]; G. Hiller and M. Schmaltz, Phys. Rev. D **90** (2014) 054014 [[arXiv:1408.1627](#) [hep-ph]]; B. Gripaios, M. Nardecchia and S. A. Renner, JHEP **1505** (2015) 006 [[arXiv:1412.1791](#) [hep-ph]].

- S. Sahoo and R. Mohanta, Phys. Rev. D **91** (2015) no.9, 094019 [[arXiv:1501.05193](#) [hep-ph]]; D. Becirevic, S. Fajfer and N. Konik, Phys. Rev. D **92** (2015) no.1, 014016 [[arXiv:1503.09024](#) [hep-ph]]; L. Calibbi, A. Crivellin and T. Ota, Phys. Rev. Lett. **115**, 181801 (2015) doi:10.1103/PhysRevLett.115.181801 [[arXiv:1506.02661](#) [hep-ph]].
- [8] A. Khodjamirian, T. Mannel, A. A. Pivovarov and Y.-M. Wang, JHEP **1009** (2010) 089 [[arXiv:1006.4945](#) [hep-ph]]; T. Hurth and F. Mahmoudi, JHEP **1404** (2014) 097 [[arXiv:1312.5267](#) [hep-ph]]; S. Descotes-Genon, L. Hofer, J. Matias and J. Virto, JHEP **1412**, 125 (2014) doi:10.1007/JHEP12(2014)125 [[arXiv:1407.8526](#) [hep-ph]]; A. Crivellin, G. D'Ambrosio and J. Heeck, Phys. Rev. D **91** (2015) no.7, 075006 [[arXiv:1503.03477](#) [hep-ph]]; M. Ciuchini, M. Fedele, E. Franco, S. Mishima, A. Paul, L. Silvestrini and M. Valli, JHEP **1606** (2016) 116 [[arXiv:1512.07157](#) [hep-ph]].
- [9] L. Randall and R. Sundrum, Phys. Rev. Lett. **83** (1999) 3370 [[arXiv:hep-ph/9905221](#)]; Phys. Rev. Lett. **83** (1999) 4690 [[arXiv:hep-th/9906064](#)].
- [10] J. A. Cabrer, G. von Gersdorff and M. Quiros, New J. Phys. **12** (2010) 075012 [[arXiv:0907.5361](#) [hep-ph]].
- [11] J. A. Cabrer, G. von Gersdorff and M. Quiros, Phys. Lett. B **697** (2011) 208 [[arXiv:1011.2205](#) [hep-ph]].
- [12] J. A. Cabrer, G. von Gersdorff and M. Quiros, JHEP **1105** (2011) 083 [[arXiv:1103.1388](#) [hep-ph]].
- [13] J. A. Cabrer, G. von Gersdorff and M. Quiros, Phys. Rev. D **84** (2011) 035024 [[arXiv:1104.3149](#) [hep-ph]].
- [14] J. A. Cabrer, G. von Gersdorff and M. Quiros, Fortsch. Phys. **59** (2011) 1135 [[arXiv:1104.5253](#) [hep-ph]].
- [15] A. Carmona, E. Ponton and J. Santiago, JHEP **1110** (2011) 137 [[arXiv:1107.1500](#) [hep-ph]].
- [16] J. A. Cabrer, G. von Gersdorff and M. Quiros, JHEP **1201** (2012) 033 [[arXiv:1110.3324](#) [hep-ph]].
- [17] M. Quiros, Mod. Phys. Lett. A **30** (2015) 1540012 [[arXiv:1311.2824](#) [hep-ph]].
- [18] E. Megias, O. Pujolas and M. Quiros, JHEP **1605** (2016) 137 [[arXiv:1512.06106](#) [hep-ph]].
- [19] E. Megias, O. Pujolas and M. Quiros, [arXiv:1512.06702](#) [hep-ph].

- [20] M. A. Luty and T. Okui, JHEP **0609** (2006) 070 [[arXiv:hep-ph/0409274](#)].
- [21] D. B. Kaplan, Nucl. Phys. B **365** (1991) 259; Y. Grossman and M. Neubert, Phys. Lett. B **474** (2000) 361 [[arXiv:hep-ph/9912408](#)]; T. Gherghetta and A. Pomarol, Nucl. Phys. B **586** (2000) 141 [[arXiv:hep-ph/0003129](#)]; S. J. Huber and Q. Shafi, Phys. Lett. B **498** (2001) 256 [[arXiv:hep-ph/0010195](#)]; S. J. Huber, Nucl. Phys. B **666** (2003) 269 [[arXiv:hep-ph/0303183](#)].
- [22] G. Panico and A. Wulzer, Lect. Notes Phys. **913** (2016) [[arXiv:1506.01961](#) [hep-ph]].
- [23] R. Barbieri, D. Buttazzo, F. Sala, D. M. Straub and A. Tesi, JHEP **1305** (2013) 069 [[arXiv:1211.5085](#) [hep-ph]]; R. Barbieri, D. Buttazzo, F. Sala and D. M. Straub, JHEP **1207** (2012) 181 [[arXiv:1203.4218](#) [hep-ph]]; M. Redi, Eur. Phys. J. C **72** (2012) 2030 [[arXiv:1203.4220](#) [hep-ph]]; G. Panico and A. Pomarol, JHEP **1607** (2016) 097 [[arXiv:1603.06609](#) [hep-ph]].
- [24] G. Buchalla, A. J. Buras and M. E. Lautenbacher, Rev. Mod. Phys. **68** (1996) 1125 [[arXiv:hep-ph/9512380](#)].
- [25] UT_{fit} Collaboration, <http://www.utfit.org/UTfit/ResultsWinter2016NP>
- [26] G. Isidori, Y. Nir and G. Perez, Ann. Rev. Nucl. Part. Sci. **60** (2010) 355 [[arXiv:1002.0900](#) [hep-ph]]; G. Isidori, [arXiv:1507.00867](#) [hep-ph].
- [27] M. E. Peskin and T. Takeuchi, Phys. Rev. D **46** (1992) 381.
- [28] R. Barbieri, A. Pomarol, R. Rattazzi and A. Strumia, Nucl. Phys. B **703** (2004) 127 [[arXiv:hep-ph/0405040](#)].
- [29] K. A. Olive *et al.* [Particle Data Group Collaboration], Chin. Phys. C **38** (2014) 090001.
- [30] G. Aad *et al.* [ATLAS Collaboration], Phys. Rev. D **90** (2014) no.5, 052005 [[arXiv:1405.4123](#) [hep-ex]].
- [31] The ATLAS collaboration, ATLAS-CONF-2015-070.
- [32] S. Chatrchyan *et al.* [CMS Collaboration], Phys. Rev. Lett. **111** (2013) no.21, 211804 Erratum: [Phys. Rev. Lett. **112** (2014) no.11, 119903] [[arXiv:1309.2030](#) [hep-ex]].
- [33] G. Aad *et al.* [ATLAS Collaboration], JHEP **1508** (2015) 148 [[arXiv:1505.07018](#) [hep-ex]].
- [34] B. Lillie, L. Randall and L. T. Wang, JHEP **0709** (2007) 074 [[arXiv:hep-ph/0701166](#)].

- [35] R. Contino, A. Pomarol and R. Rattazzi, unpublished work; See talks by R. Rattazzi at Planck 2010 [[indico/contribId=163&confId=75810](#)], and by A. Pomarol at the XVI IFT Xmas Workshop 2010 [<http://www.ift.uam-csic.es/workshops/Xmas10/doc/pomarol.pdf>]
- [36] B. Bellazzini, C. Csaki, J. Hubisz, J. Serra and J. Terning, Eur. Phys. J. C **74**, 2790 (2014) [[arXiv:1305.3919](#) [hep-th]].
- [37] F. Coradeschi, P. Lodone, D. Pappadopulo, R. Rattazzi and L. Vitale, JHEP **1311**, 057 (2013) [[arXiv:1306.4601](#) [hep-th]].
- [38] E. Megias and O. Pujolas, JHEP **1408**, 081 (2014) [[arXiv:1401.4998](#) [hep-th]].